ACCSCIENCE PUBLISHING

Eurasian Journal of Medicine and Oncology

ORIGINAL RESEARCH ARTICLE

Investigating the role of *TIMM8B* in lung adenocarcinoma: Expression patterns, prognostic value, and therapeutic implications

Zhuli Zheng[1†], Libao Gong[1†], Hongcheng Zhong[2†], Bingjiang Huang[1], Yunyan Cong[1], Beilong Zhong[2*], and Zhihui Wang[1*]

[1]Department of Thoracic Oncology, The Fifth Affiliated Hospital of Sun Yat-sen University, Zhuhai, China

[2]Department of Thoracic Surgery, The Fifth Affiliated Hospital of Sun Yat-sen University, Zhuhai, China

Abstract

Introduction: Translocase of inner mitochondrial membrane 8 homolog B (*TIMM8B*) is crucial for mitochondrial function, but its role in lung adenocarcinoma (LUAD) remains underexplored.

Objective: This study investigates *TIMM8B* expression patterns, prognostic value, and potential therapeutic implications in LUAD.

Methods: The expression and prognostic potential of *TIMM8B* in LUAD were analyzed using data from The Cancer Genome Atlas (TCGA), Genotype-Tissue Expression, Gene Expression Omnibus, and Gene Expression Profiling Interactive Analysis 2, with survival analysis performed through Kaplan–Meier plotter. The prognostic value was validated using a LUAD tissue microarray and a nomogram. *TIMM8B*-related differentially expressed genes were identified using TCGA and LinkedOmics, and were functionally annotated using the Gene Ontology and Kyoto Encyclopedia of Genes and Genomes databases. Immunological features were assessed using TCGA data through the XCELL and tumor immune dysfunction and exclusion algorithms. Associations among *TIMM8B*, m6A modification, ferroptosis-related genes, and tumor genetic mutations were analyzed using TCGA data. Drug response correlations were explored using the Genomics of Drug Sensitivity in Cancer and Comparative Toxicogenomics databases. *TIMM8B*-depleted LUAD cell lines were analyzed using ribonucleic acid sequencing and subjected to cell cycle analysis.

Results: *TIMM8B* is overexpressed in multiple cancers, including LUAD. High *TIMM8B* expression correlates with poorer overall survival in LUAD. A nomogram incorporating *TIMM8B* and pathological tumor-node-metastasis stage showed reliable predictive performance. *TIMM8B*-related gene analyses suggest roles in cell adhesion, chromosome segregation, and critical cancer pathways. *TIMM8B* shapes an immunosuppressive tumor microenvironment in LUAD, affecting immune cell infiltration and immunotherapy response. Elevated *TIMM8B* expression is associated with *TP53* mutations and chemotherapy resistance. Knockdown of *TIMM8B* in H1299 cells downregulates PD-L1, induces G1 phase arrest, and triggers a chemokine (C-C motif) ligand 2-mediated inflammatory response, highlighting roles in cell cycle regulation and inflammatory pathways.

†These authors contributed equally to this work.

***Corresponding authors:**
Beilong Zhong (beilongzhuhai@hotmail.com);
Zhihui Wang (wangzhh33@mail.sysu.edu.cn)

Citation: Zheng Z, Gong L, Zhong H, *et al*. Investigating the role of *TIMM8B* in lung adenocarcinoma: Expression patterns, prognostic value, and therapeutic implications. *Eurasian J Med Oncol*. 2026;10(4):025180152. doi: 10.36922/EJMO025180152

Received: April 28, 2025

Revised: June 1, 2025

Accepted: June 24, 2025

Published online: August 25, 2025

Conclusion: These findings underscore *TIMM8B*'s multifaceted role in cancer progression and its potential as a prognostic marker and therapeutic target in LUAD.

Keywords: Translocase of inner mitochondrial membrane 8 homolog B; Prognosis; Immunotherapy; Inflammatory; Lung adenocarcinoma

1. Introduction

In 2022, lung cancer was the leading cause of cancer morbidity and mortality, with nearly 2.5 million new cases and over 1.8 million deaths worldwide.[1] Among non-small cell lung cancer cases, lung adenocarcinoma (LUAD) is the most prevalent subtype.[2] In recent years, the treatment of LUAD has incorporated multiple modalities, including surgery, radiation therapy, chemotherapy, targeted therapy, and immune checkpoint inhibitors. These interventions, individually or in combination, have notably prolonged survival in patients with LUAD. However, despite treatment advancements, the 5-year overall survival (OS) rate for advanced-stage LUAD patients remains around 20–30%.[2,3] This poor prognosis is primarily attributed to over 50% of LUAD patients being diagnosed with metastatic disease.[4] While tumor stage is crucial for guiding treatment decisions and predicting prognosis in LUAD, it alone does not fully account for patient variability. Consequently, there is still a notable absence of reliable prognostic factors in this disease.

Mitochondrial dysfunction, recognized as a hallmark of cancer cells, disrupts cellular metabolism and plays a pivotal role in tumor development. Consequently, it has become a central target in cancer therapy.[5] Translocase of the inner mitochondrial membrane (TIMM) proteins are responsible for forming transport channels within the inner membrane of mitochondria.[6] This protein-transporting system, in which the TIMM proteins play significant roles, is essential for the proper mitochondrial function.[7] The clinical significance of the TIMM family has been increasingly recognized in recent years. Multiple studies have demonstrated that TIMM17A expression was significantly correlated with tumor grade, lymph node involvement, and stage in breast cancer (BRCA) patients, as well as overall and disease-free survival.[8,9] In addition, *TIMM8A* has been implicated in BRCA as a poor prognostic factor and an oncogene.[10,11] It is also associated with immune cell dysfunction in BRCA, suggesting its potential as a predictive marker for the efficacy of anti-programmed death-ligand 1 therapy.[10,12] Translocase of inner mitochondrial membrane 8 homolog B (*TIMM8B*) protein, a member of the TIMM family involved in mitochondrial protein import, plays a crucial role in maintaining mitochondrial function and is essential for proper cellular metabolism. It is responsible for transporting proteins into the intermembrane space of mitochondria.[13] Mutations in the *TIMM8B* gene can lead to a rare X-linked disorder known as Mohr–Tranebjaerg syndrome, which is characterized by hearing loss, neurological abnormalities, and visual impairment.[14,15] However, the functional role of *TIMM8B* in cancer has been reported in only a few bioinformatics analyses.[16,17] Notably, the function and clinical significance of *TIMM8B* in LUAD have not been explored. Therefore, this study aims to investigate *TIMM8B* expression patterns, prognostic value, and potential therapeutic implications in LUAD.

2. Materials and methods

2.1. Data collection and preprocessing

Data collection and preprocessing involved obtaining ribonucleic acid (RNA)-sequencing expression profiles (level 3) and corresponding clinical data for LUAD (n = 516) and adjacent paracarcinoma tissue (n = 59) from The Cancer Genome Atlas (TCGA) dataset via the GDC data portal (https://portal.gdc.cancer.gov). Normal tissue data (n = 578) from the latest release (V8) of the Genotype-Tissue Expression (GTEx) dataset were sourced from the GTEx portal (https://www.gtexportal.org/home/datasets). RNA sequencing data originally in FPKM format were converted to TPM format and log2 transformed. In addition, microarray data from two Gene Expression Omnibus (GEO) datasets, GSE31210 (LUAD = 228, normal = 20) and GSE10072 (LUAD = 49, normal = 58), were downloaded in MINiML format from the GEO database (http://ncbi.nlm.nih.gov/geo/). Expression levels of *TIMM8B* in TCGA LUAD samples were categorized into $TIMM8B^{high}$ and $TIMM8B^{low}$ groups based on quartile thresholds: $TIMM8B^{low}$ (25th percentile) and $TIMM8B^{high}$ (75th percentile). All data processing and statistical analyses were performed using R (version 4.0.3, r-project.org) and relevant R packages.

2.2. Expression analysis of *TIMM8B* between cancer and normal tissue

To analyze the expression of *TIMM8B* across cancer and normal tissue types, we utilized RNA-sequencing data

from cancer samples sourced from the TCGA dataset. The control group comprised RNA expression profiles obtained from normal tissue samples available on the GTEx data portal. In addition, microarray data from the GSE31210 and GSE10072 datasets within the GEO database were downloaded for comparative analysis between cancer and normal tissues. Statistical differences between groups were assessed using the Mann–Whitney *U* test. Differential expression patterns were visualized using box plots.

2.3. Survival analysis of *TIMM8B* across cancer types

To comprehensively assess the prognostic significance of *TIMM8B* across multiple cancer types, we utilized the Gene Expression Profiling Interactive Analysis 2 (GEPIA2) online database (http://gepia2.cancer-pku.cn/). Specifically for LUAD, we validated *TIMM8B*'s correlation with OS using the Kaplan–Meier plotter database (http://kmplot.com/analysis/). In addition, OS differences were compared using data from the TCGA and GSE72094 datasets. Kaplan–Meier curves were generated, and statistical significance, hazard ratios (HRs) with 95% confidence intervals, and *p*-values were calculated using log-rank tests and univariate Cox proportional hazards regression analysis.

2.4. Development and validation of a nomogram for prognosis in LUAD

For LUAD, we collected 254 samples from the TCGA database and 393 samples from the GSE72094 dataset within GEO, all with comprehensive clinical and follow-up data, including demographic factors (age and gender), smoking status, and pathological stages (pathological tumor [pT], pathological node [pN], pathological metastasis [pM], and pTNM). *TIMM8B* expression levels and survival status were also included. We conducted univariate and multivariable survival analyses to evaluate *TIMM8B*'s prognostic role. The TCGA LUAD dataset was randomly divided into training and internal validation cohorts (7:3 ratio), with the GSE72094 dataset serving as the external validation cohort. Categorical variables were analyzed using Chi-squared or Fisher's exact tests in univariate analysis. Multivariate analysis was performed using LASSO logistic regression to identify independent risk factors and construct a prognostic nomogram for survival status prediction. Nomogram performance was assessed using receiver operating characteristic (ROC) curves, calibration curves (evaluating the nomogram's predictive accuracy), and decision curve analysis to determine clinical usefulness. Statistical analyses utilized R software version 4.2.2 and additional tools, including MSTATA software (www.mstata.com), supported by R packages such as "survival," "survminer," "dcurves," "ggalluvial," "ggplot2," "rms," and "rmda."

2.5. Analysis of *TIMM8B*-related differentially expressed genes and functional enrichment in LUAD

Differential expression analysis was performed between *TIMM8B*^{high} and *TIMM8B*^{low} groups in TCGA LUAD, as well as between LUAD and normal tissue from the GSE43458 dataset, using the R package "limma." Criteria for differential expression were defined as "Adjusted $p<0.05$ and $|\text{Log2 (Fold Change)}| > 1$." To identify co-expressed genes of *TIMM8B* in LUAD, Pearson correlation analysis was conducted using the LinkedOmics database (http://www.linkedomics.org/). Results from both differential expression and co-expression analyses were visualized using volcano plots. In addition, Venn diagrams were created to explore intersecting genes between the two analyses, utilizing R packages "VennDiagram" and "ggplot2." Functional enrichment analyses were carried out to gain insights into the biological functions of the intersecting genes, utilizing Gene Ontology (GO) and Kyoto Encyclopedia of Genes and Genomes (KEGG) pathways. The "clusterProfiler" R package was employed for these analyses.

2.6. Analysis of *TIMM8B*-related immunological features and predictive value of immunotherapy in LUAD

To assess immune scores reliably, we utilized the R package "XCELL" to compute immunological features within the tumor microenvironment (TME) of TCGA samples. Initially, Spearman coefficients were employed to identify immune cells correlated with *TIMM8B* expression. The differential abundance of immune cells between the *TIMM8B*^{high} and *TIMM8B*^{low} groups was compared using the Wilcoxon test.

The potential response to immune checkpoint blockade was predicted using the tumor immune dysfunction and exclusion (TIDE) algorithm[18] for both *TIMM8B*^{high} and *TIMM8B*^{low} groups. The predictive value of *TIMM8B* expression for OS with anti-programmed cell death protein 1 (PD1) or anti-cytotoxic T-lymphocyte associated protein 4 (CTLA4) immunotherapy was evaluated and visualized using the Kaplan–Meier method with the log-rank test (http://kmplot.com/analysis/).

2.7. Correlation analysis of *TIMM8B* with m6A- and ferroptosis-related genes in LUAD

To investigate the influence of *TIMM8B* expression (*TIMM8B*^{high} and *TIMM8B*^{low}) on m6A modifications and its potential interaction with ferroptosis in TCGA LUAD, Spearman correlation coefficients were computed between *TIMM8B* and m6A- and ferroptosis-related genes. The list of m6A-related genes used in this study was sourced

from the study by Li *et al.*[19] on molecular characterization and clinical significance of m6A modulators across 33 cancer types. Ferroptosis-related genes were extracted from the systematic analysis by Liu *et al.*[20] on ferroptosis in cancer, as cataloged in the FerrDb database (http://www.zhounan.org/ferrdb/current/), and categorized as drivers, suppressors, and markers. Visualization of correlation results was performed using the R package "ggplot2," and a multi-gene correlation plot was generated using "pheatmap" in R. To explore the influence of *TIMM8B* on these genes further, gene set enrichment analysis (GSEA) was conducted using gene sets obtained from the FerrDb database. Visualization of GSEA results was facilitated through an online platform (https://www.bioinformatics.com.cn).

2.8. Correlation analysis of *TIMM8B* with gene mutation profiles in LUAD

RNA-sequencing expression profiles of *TIMM8B* and genetic mutation data for LUAD were obtained from the TCGA dataset. Mutation data were processed and visualized using the "maftools" package in R. To investigate common gene mutation profiles in LUAD, including *TP53*, *KRAS*, *EGFR*, *KEAP1*, and *STK11*, we analyzed two groups of LUAD samples ($TIMM8B^{high}$ and $TIMM8B^{low}$) from TCGA. Mutation annotation format files for these genes were downloaded and processed. The mutation profiles of *TP53*, *KRAS*, *EGFR*, and *STK11*, along with *TIMM8B* expression, were extracted from the GSE72094 dataset, which can be sourced from clinical data in the GEO dataset.

2.9. Correlation analysis between *TIMM8B* and drug sensitivity in LUAD

To explore potential therapeutic implications of *TIMM8B* in LUAD, we examined its correlation with drug responses using IC_{50} data obtained from the Genomics of Drug Sensitivity in Cancer (GDSC) database (https://www.cancerrxgene.org/). We investigated the relationship between *TIMM8B* expression levels and IC_{50} values of various drugs, including small-molecule target drugs and common chemotherapeutic agents. In addition, we conducted a stemness feature analysis using the one-class logistic regression machine learning algorithm to calculate messenger RNA stemness index (mRNAsi), as proposed by Malta *et al.*[21] The Spearman correlation method was applied to analyze RNA expression data. To predict potential associations between *TIMM8B* and chemicals, we utilized the Comparative Toxicogenomics Database (CTD) (https://ctdbase.org/), which integrates chemistry, genes, phenotypes, diseases, and environmental factors. For viewing molecular structures of relevant drugs, the PubChem database (https://pubchem.ncbi.nlm.nih.gov/) was consulted. We used Autodock Vina 1.2.2, a protein-ligand docking software,[22] to analyze binding affinities and interaction modes between candidate drugs and *TIMM8B*. Molecular structures of drugs were retrieved from PubChem Compound, and *TIMM8B*'s 3D coordinates were obtained from the Protein Data Bank (PDB) (http://www.rcsb.org/pdb/home/home.do).[23] Before docking analysis, the *TIMM8B* protein and drug molecular files were formatted into PDBQT format by excluding water molecules and adding polar hydrogen atoms. Docking simulations were performed using Autodock Vina 1.2.2. Throughout the analysis, we utilized R software with packages including "reshape2," "ggpubr," "ggplot2," "pRRophetic," and "corrplot" for data manipulation, visualization, and correlation analysis.

2.10. Tissue microarray (TMA) and immunohistochemical staining analysis

LUAD TMA samples, comprising 80 tumor tissues and 79 corresponding paracancerous tissues, were obtained from Superbiotek (LUC1601, Superbiotek, China). Informed consent was obtained from all participants. Pathological confirmation verified that all 80 tumor tissue samples were LUAD, whereas the adjacent tissue specimens were normal. Comprehensive data, including clinical information, pathology details, and follow-up data, were obtained for all cases.

TIMM8B protein expression was assessed using immunohistochemistry. Tissue sections were prepared by dewaxing and rehydrating samples, followed by blocking with a milk solution for 5 min. The sections were then incubated overnight at 4°C with a primary antibody against the *TIMM8B* protein (1:500; BS72767, Bioworld Technology, China). After washing with phosphate-buffered solution (PBS), a fluorescently labeled secondary antibody was applied and incubated at 37°C for 30 min, followed by additional PBS washes. Subsequently, diaminobenzidine was applied, and the sections were counterstained with hematoxylin. Tissue sections were dehydrated using an ethanol gradient and mounted with neutral gum. After staining, TMAs were digitized using Panoramic Viewer (NDP viewer software, Japan).

Staining results for *TIMM8B* were independently evaluated by three pathologists blinded to clinical features. Evaluation involved quantifying staining scores based on both the percentage of positive cells and staining intensity:

- Percentage of positive cells: 0 (0%), 1 (1–25%), 2 (26–50%), 3 (51–75%), or 4 (≥76%)
- Staining intensity: 0 (No staining), 1 (Weak), 2 (Moderate), or 3 (Strong).

The final *TIMM8B* immunostaining score was computed by summing the scores of the percentage

of positive cells and staining intensity. High *TIMM8B* expression was defined as the top quartile of the final score, whereas low expression was defined as the bottom quartile.

2.11. Cell lines and culture

Six human adenocarcinoma cell lines (H1299, HCC827, A549, H1975, H1563, and H460) were generously provided by Professor Zhangli from the Cancer Center of Sun Yat-sen University. These cells were cultured in RPMI Medium 1640 or Dulbecco's Modified Eagle Medium, supplemented with 10% fetal bovine serum from Gibco (USA). Cultivation was conducted in a humidified incubator at 37°C with 5% CO_2.

2.12. Lentiviral H1299/*shTIMM8B* construction

Small hairpin RNAs (shRNAs) targeting the human *TIMM8B* gene were designed by GENE *DENOVO* (China). Lentivirus lacking shRNA served as the control. The sh*TIMM8B* fragments were integrated into the lentivirus vector and transfected into 293T cells, along with packaging vectors, using Lipofectamine 3000 (Invitrogen, United States of America [USA]) at 70–80% cell density. After lentivirus construction, cells were transfected to establish H1299 cells with *TIMM8B* knockdown. Recombinant lentivirus was harvested from the culture medium 48 h post-transfection for subsequent infection. Knockdown efficiency was confirmed via Western blot analysis. For RNA isolation and reverse transcription quantitative polymerase chain reaction (RT-qPCR), total RNA was extracted using Trizol reagent (Vazyme, China), followed by RT-qPCR using Hieff® qPCR SYBR Green Master (Yeasen, China). Primer sequences were as follows: *TIMM8B* forward, 5′-AAGCCGATGAAGCGGAGTTG-3′, reverse, 5′-CCCTGGCTTCTCCACACATT-3′; GAPDH forward, 5′-AGAAGGCTGGGGCTCATTTG-3′, reverse, 5′-AGGGGCCATCCACAGTCTTC-3′. Relative messenger RNA (mRNA) expression (*TIMM8B*/GAPDH) was determined using the comparative Ct method ($2^{-\Delta\Delta Ct}$).

2.13. Western blotting

Total cellular protein was extracted using RIPA lysis buffer (Beyotime, China) supplemented with protease inhibitors (KeyGene, China). Protein concentration was determined using the BCA Protein Assay Kit (Beyotime, China). Twenty micrograms of protein lysates were separated using 8–12% sodium dodecyl sulfate polyacrylamide gel electrophoresis and transferred onto polyvinylidene fluoride membranes. Membranes were blocked with 5% non-fat milk for 1 h at room temperature, then incubated overnight at 4°C with primary antibodies. Afterward, membranes were incubated with goat anti-rabbit immunoglobulin G polyclonal antibody (1:3000; Thermo Fisher Scientific, USA) labeled with horseradish peroxidase at room temperature for 2 h. Protein signals were visualized using the chemiluminescence ECL-PLUS kit (Tanon, China).

2.14. Flow cytometry for cell cycle analysis

For cell cycle analysis, treated cells were centrifuged for 5 min, washed sequentially with PBS and ×1 binding buffer, and fixed in 70% ethanol for ≥1 h. Cells were stained with PI (Sigma, Germany) and analyzed using flow cytometry to determine the proportions in G1, S, and G2 phases in both vector and sh*TIMM8B* groups.

2.15. RNA sequencing and bioinformatics analysis

Total RNA extraction was performed using the Trizol reagent kit (Invitrogen, USA) according to the manufacturer's protocol. RNA integrity was assessed using an Agilent 2100 Bioanalyzer (Agilent Technologies, USA) and confirmed using RNase-free agarose gel electrophoresis. Eukaryotic mRNA enrichment utilized Oligo (dT) beads from the Ribo-Zero™ Magnetic Kit (Epicentre, USA). Subsequently, mRNA underwent fragmentation and reverse transcription into cDNA using the NEBNext Ultra RNA Library Prep Kit for Illumina (NEB #7530, New England Biolabs, USA). Double-stranded cDNA fragments were subjected to end repair, A-tailing, and ligation to Illumina sequencing adapters. Ligation products were purified using AMPure XP beads (1.0×; Beckman Coulter, USA) and subsequently PCR-amplified. The resulting cDNA library was sequenced using an Illumina Novaseq6000 sequencer (Gene Denovo Biotechnology Co., China).

DESeq2 software was used to analyze differential gene expression between H1299/sh*TIMM8B* and H1299/control groups. Genes with a false discovery rate (FDR) <0.05 and an absolute fold change ≥2 were considered differentially expressed genes (DEGs).

The GO and KEGG pathway analyses were performed to explore the biological significance of DEGs. In addition, GSEA using GSEA software and MSigDB was conducted to identify significant differences in GO terms and KEGG pathways between groups.

STRING v10 was utilized to construct protein–protein interaction networks, with genes represented as nodes and interactions as edges. The network was visualized using Cytoscape (v3.7.1; https://cytoscape.org/) software to elucidate core and hub gene interactions.

2.16. Statistical analysis

Statistical analyses were conducted using IBM Statistical Package for Social Sciences version 25.0 (USA). Data are presented as the mean ± standard error of the mean. The

Mann–Whitney U-test was used for comparisons between two groups, whereas the Chi-squared test analyzed the relationship between *TIMM8B* protein expression and clinicopathological parameters. Survival analysis was performed using Kaplan–Meier analysis with the log-rank test. Cox proportional hazards models were used for multivariate analysis to assess the prognostic significance of *TIMM8B* in LUAD. Statistical significance was defined as $p<0.05$.

3. Results

3.1. Expression analysis of *TIMM8B* across cancer types

In a pancancer analysis covering 33 types of tumors (Figure 1A), *TIMM8B* mRNA expression was significantly elevated in multiple cancers, including BRCA, bladder urothelial carcinoma, cholangiocarcinoma, colon adenocarcinoma, esophageal carcinoma, glioblastoma multiforme, kidney renal papillary cell carcinoma, kidney renal clear cell carcinoma, liver hepatocellular carcinoma (LIHC), LUAD, lung squamous cell carcinoma, rectum adenocarcinoma, prostate adenocarcinoma, stomach adenocarcinoma, and uterine corpus endometrial carcinoma, compared to normal tissues ($p<0.05$). Conversely, *TIMM8B* exhibited lower expression in kidney chromophobe, pheochromocytoma, and paraganglioma.

Focusing specifically on TCGA LUAD samples ($n = 516$) versus normal controls ($n = 637$) from the GTEx database (Figure 1B), *TIMM8B* showed significant upregulation in LUAD tissues. This differential expression pattern was consistently observed in the GSE10072 (Figure S1A) and GSE31210 (Figure S1B) datasets, further confirming elevated *TIMM8B* expression in LUAD compared to normal lung tissues. Collectively, these findings underscore the potential distinct role of *TIMM8B* in LUAD pathogenesis, suggesting its relevance as a biomarker or therapeutic target in this cancer type.

3.2. Prognostic analysis of *TIMM8B* across cancer types

Prognostic analysis of *TIMM8B* across different types of cancers was conducted by categorizing samples into $TIMM8B^{high}$ and $TIMM8B^{low}$ groups. Using the GEPIA2 database encompassing 33 tumor types (Figure S2), the analysis revealed that elevated *TIMM8B* expression was correlated with poorer OS in adrenocortical carcinoma (ACC), LIHC, uveal melanoma (UVM), and LUAD. Conversely, high *TIMM8B* expression was associated with favorable OS in ovarian serous cystadenocarcinoma (OV) ($p<0.05$), indicating a multifaceted role of *TIMM8B* across various tumor types influenced by their distinct microenvironments. Given the significant impact of *TIMM8B* on LUAD prognosis observed in the pancancer analysis, further survival analysis was performed using four distinct LUAD cohorts: GEPIA2, Kaplan–Meier plotter, TCGA, and GSE72094. These cohorts included 240, 1,161, 254, and 398 samples, respectively. Kaplan–Meier analysis conducted on GEPIA2 (Figure 2A) and Kaplan–Meier plotter (Figure 2B) datasets consistently demonstrated a negative correlation between *TIMM8B* expression and OS in LUAD patients, with log-rank test $p=0.019$ and

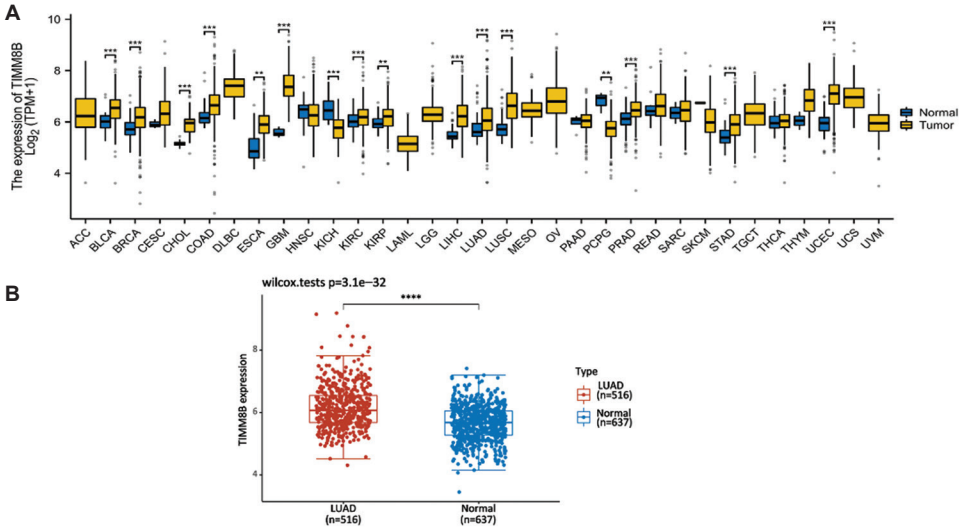

Figure 1. Differential expression analysis of translocase of inner mitochondrial membrane 8 homolog B (*TIMM8B*) in normal and tumor tissues using the Mann–Whitney *U*-test. (A) Expression levels of *TIMM8B* across 33 cancer types and 24 corresponding paracancerous tissues from the Cancer Genome Atlas (TCGA) database. (B) Comparison of *TIMM8B* expression levels in normal and tumor tissues from the Genotype-Tissue Expression and TCGA lung adenocarcinoma databases. Statistical significance is indicated by * for $p<0.05$, ** for $p<0.01$, and *** or **** for $p<0.001$.

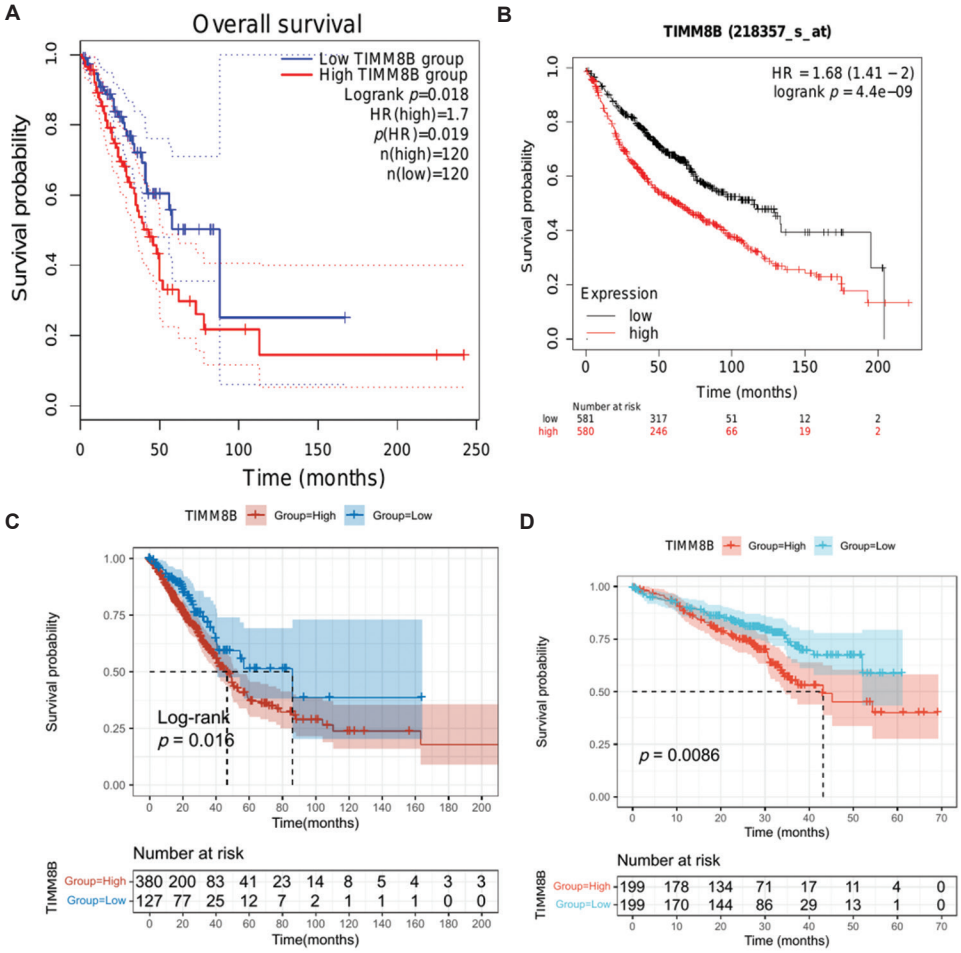

Figure 2. Survival analysis of *TIMM8B* expression on OS in LUAD. (A) Survival analysis on OS in LUAD (n = 240) using Gene Expression Profiling Interactive Analysis 2 data, focusing on *TIMM8B* expression. (B) *TIMM8B* expression and survival analysis in LUAD using mRNA RNA-seq data from the Kaplan–Meier plotter (n = 1,161). (C) Survival analysis of *TIMM8B* expression on OS in LUAD (n = 254) using the Cancer Genome Atlas data. (D) Survival analysis of *TIMM8B* expression on OS in LUAD (n = 398) using GSE72094 data. The 95% confidence interval curves are shown with dotted lines.
Abbreviations: HR: Hazard ratio; OS: Overall survival; *TIMM8B:* Translocase of inner mitochondrial membrane 8 homolog B; LUAD: Lung adenocarcinoma; mRNA: Messenger RNA.

4.4×10^{-9}, respectively. Similarly, analyses of TCGA LUAD (Figure 2C; p=0.012) and GSE72094 (Figure 2D; p=0.0086) profiles confirmed that high *TIMM8B* expression was marginally associated with poorer prognosis in LUAD. These findings underscore the potential significance of *TIMM8B* as a prognostic biomarker in LUAD, suggesting its role in influencing disease progression and patient outcomes. Further research is warranted to elucidate the underlying mechanisms through which *TIMM8B* contributes to LUAD pathogenesis and its implications for therapeutic strategies.

3.3. Clinicopathological characteristics and independent prognostic value of *TIMM8B* in LUAD

In the analysis of *TIMM8B* mRNA expression and its clinicopathological implications in LUAD, we utilized the TCGA LUAD dataset comprising 254 samples categorized into $TIMM8B^{high}$ and $TIMM8B^{low}$ groups. Analysis revealed significant associations of *TIMM8B* expression with key clinicopathological parameters (Table 1): pT_stage (p<0.001), pN_stage (p = 0.003), pTNM_stage (p = 0.018), and patient age (p = 0.044). However, no correlations were found with gender (p = 0.612), smoking status (p = 0.368), or pM_stage (p = 0.974). These findings underscore *TIMM8B*'s potential as a biomarker for poor prognosis in LUAD, particularly to age and tumor stage. To further elucidate *TIMM8B*'s independent prognostic significance in LUAD, we conducted univariate and multivariate Cox proportional hazard analyses using both TCGA LUAD and GSE72094 datasets. The forest plot (Figure 3) illustrates the outcomes of these analyses. In TCGA LUAD (Figure 3A), univariate and multivariate analyses demonstrated that

Table 1. Patient demographics and baseline characteristics in the Cancer Genome Atlas LUAD dataset

Characteristic	*TIMM8B*		*p*-value[b]
	Low (*n*=127)[a] (%)	High (*n*=127)[a] (%)	
Age			
≤60	34 (27)	49 (40)	0.044
>60	90 (73)	75 (60)	
Unknown	3	3	
Gender			
Female	74 (58)	70 (55)	0.612
Male	53 (42)	57 (45)	
Smoking			
Yes	107 (86)	101 (82)	0.368
No	17 (14)	22 (18)	
Unknown	3	4	
pT_stage			
T1	61 (48)	29 (23)	<0.001
T2	47 (37)	78 (61)	
T3	13 (10)	15 (12)	
T4	5 (4)	5 (4)	
Unknown	1	0	
pN_stage			
N0	95 (76)	71 (56)	0.003
N1	17 (14)	28 (22)	
N2	12 (10)	27 (21)	
N3	1 (1)	0 (0)	
Unknown	2	1	
pM_stage			
M0	117 (94)	119 (94)	0.974
M1	8 (6)	8 (6)	
Unknown	2	0	
pTNM_stage			
I	76 (61)	61 (48)	0.018
II	29 (23)	27 (21)	
III	12 (10)	31 (24)	
IV	8 (6)	8 (6)	
Unknown	2	0	

Notes: [a]Data expressed as *n* (%); [b]Pearson's Chi-squared test or Fisher's exact test.
Abbreviation: pTNM: Pathological tumor-node-metastasis.

TIMM8B expression, along with pT_stage, pN_stage, pM_stage, and pTNM_stage, significantly influenced OS. Multivariate analysis confirmed *TIMM8B* expression, pT_stage, and pTNM_stage as independent prognostic factors for OS. Similarly, in the GSE72094 dataset (Figure 3B), both univariate and multivariate analyses indicated significant impacts of *TIMM8B* expression, pT_stage, pN_stage, and pTNM_stage on OS, with multivariate analysis confirming *TIMM8B* expression, pN_stage, and pTNM_stage as independent prognostic factors. In summary, these findings highlight *TIMM8B*'s robust independent prognostic value in LUAD, emphasizing its potential utility as a prognostic biomarker and its implications for therapeutic stratification in clinical practice.

3.4. Development and validation of a nomogram incorporating *TIMM8B* for prognostic evaluation in LUAD

To develop a prognostic nomogram incorporating *TIMM8B* for LUAD, we utilized samples from TCGA LUAD (n = 254) and GSE72094 (n = 398) datasets, which were divided into training, internal test, and external test cohorts. Table 2 summarizes the baseline characteristics of these cohorts, revealing significant differences in age, pT_stage, and pN_stage distributions among them. These variations underscore the importance of accounting for heterogeneity in subsequent analyses. Initially, candidate predictors including age, gender, smoking, pT_stage, pN_stage, pM_stage, pTNM_stage, and *TIMM8B* expression were considered. Using LASSO regression in the training cohort, these predictors were reduced to two potential variables, as depicted in Figure 4A. The cross-validated error plot (Figure 4B) identified a model with minimal error, including *TIMM8B* expression level and pTNM_stage as independent predictors. Subsequent ROC analysis (Figure 4C) validated the predictive performance of the model, with area under the curve (AUC) values exceeding 0.5 for both variables. Based on these findings, a simplified nomogram integrating *TIMM8B* expression level and pTNM stage was constructed (Figure 4D). This nomogram allows a straightforward prediction of survival outcomes in LUAD patients. The nomogram's performance was evaluated across different cohorts, demonstrating consistent AUC values (Figure 4E). Calibration plots (Figure 4F) further confirmed the nomogram's reliability, showing strong agreement between predicted and observed survival probabilities in the training cohort. Decision curve analysis (Figure 4G) illustrated the clinical utility of the nomogram, indicating substantial net benefit across a range of threshold probabilities. This analysis underscores the nomogram's potential for informing clinical decisions and improving patient outcomes in LUAD. In conclusion, the developed nomogram integrating *TIMM8B* expression level and pTNM stage represents a valuable tool for prognostication in LUAD, offering reliable predictions and supporting personalized treatment strategies in clinical practice.

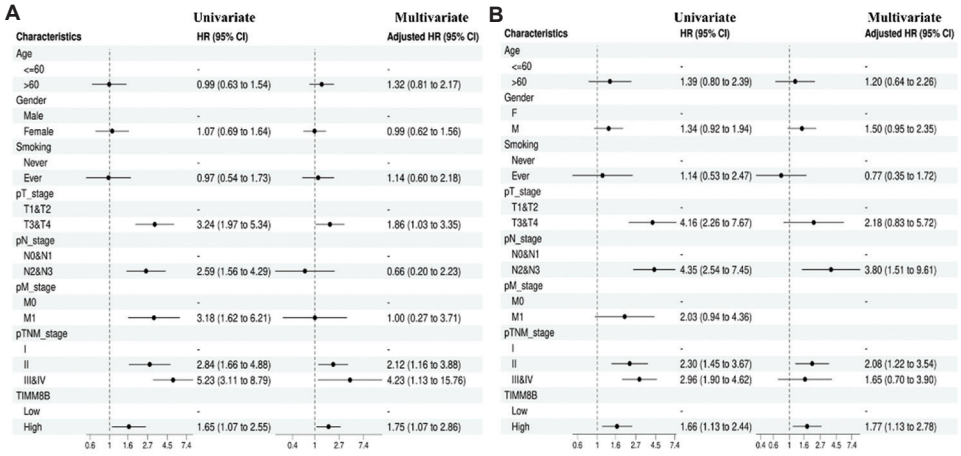

Figure 3. Univariate and multivariate Cox proportional analyses in LUAD. (A) Forest plot showing univariate and multivariate Cox analysis for OS in the Cancer Genome Atlas LUAD (n = 254). (B) Forest plot showing univariate and multivariate Cox analysis for OS in LUAD using GSE72094 data (n = 398). Abbreviations: CI: Confidence interval; HR: Hazard ratio; OS: Overall survival; LUAD: Lung adenocarcinoma.

3.5. Analysis of *TIMM8B*-related genes and the biological function of *TIMM8B* in LUAD

To delve into the underlying pathogenic mechanisms involving *TIMM8B* in LUAD, we initiated our investigation by screening co-expressed genes using the TCGA LUAD dataset via the LinkedOmics database (Figure S3A). This analysis identified 2992 genes positively correlated and 3546 genes negatively correlated with *TIMM8B* expression in LUAD ($|cor| > 0.2$, FDR < 0.05). Concurrently, differential expression analysis in the GEO GSE43458 dataset revealed 2,663 genes that were significantly altered between LUAD (n = 80) and normal lung tissues (n = 30), comprising 898 upregulated and 1765 downregulated protein-coding genes (Figure S3B). Further characterization of *TIMM8B*-associated genes in TCGA LUAD identified 2,557 DEGs between $TIMM8B^{high}$ and $TIMM8B^{low}$ samples, with 1,310 genes upregulated and 1,247 genes downregulated (Figure S3C). Integrating these datasets, we identified 429 genes that overlapped between *TIMM8B* co-expressed genes and *TIMM8B*-associated DEGs (Figure 5A), consisting of 145 upregulated and 284 downregulated genes. Subsequent functional enrichment analyses of these 429 overlapping genes provided insights into their potential biological roles in LUAD. GO analyses revealed enrichment in biological processes such as nuclear division, chromosome segregation, mitotic nuclear division, cell–matrix adhesion, and cell–substrate adhesion (Figure 5B). Molecular function terms highlighted activities such as histone kinase activity, cyclin-dependent protein serine, and extracellular matrix (ECM) structural constituent (Figure 5B). Cellular component terms were enriched in chromosomal regions and collagen-containing ECM (Figure 5B). Moreover, KEGG pathway analyses indicated significant involvement of *TIMM8B*-related genes in pathways critical for cancer progression, including the cell cycle, p53 signaling pathway, and ECM–receptor interaction (Figure 5C). Additional pathways such as cell adhesion molecules, cellular senescence, and metabolic regulation pathways (e.g., biosynthesis of amino acids and carbon metabolism) were also implicated, suggesting diverse roles for *TIMM8B* in LUAD pathogenesis. Overall, these findings underscore the multifaceted involvement of *TIMM8B* and its associated genes in biological processes and pathways crucial for LUAD development and progression, providing a foundation for further mechanistic and therapeutic investigations in this context.

3.6. Immunosuppressive TME shaped by *TIMM8B* in LUAD

To explore *TIMM8B*'s role in immune regulation in LUAD, we utilized the XCELL database to assess its impact on the TME. Our analysis revealed that *TIMM8B* positively correlates with common lymphoid progenitors, $CD4^+$ Th2 cells, and M1 macrophages, while showing a negative association with regulatory T cells, various T cell subsets (including $CD4^+$ central memory, $CD4^+$ effector memory, $CD4^+$ naive, and $CD8^+$ cells), myeloid dendritic cells, B cell subsets (memory, plasma, and class-switched memory B cells), granulocyte–monocyte progenitors, mast cells, hematopoietic stem cells, and endothelial cells (Figure S4). *TIMM8B* also negatively correlated with stroma score, microenvironment score, and immune score. Comparison of $TIMM8B^{high}$ versus $TIMM8B^{low}$ groups demonstrated reduced infiltration of immune cells, particularly $CD8^+$ and various $CD4^+$ cell subtypes (Figure S4). Interestingly, the $TIMM8B^{high}$ group showed increased levels of $CD4^+$

Table 2. Patient demographics and baseline characteristics from the Cancer Genome Atlas LUAD and GSE72094 datasets

Characteristic	Training cohort (*n*=178)[a] (%)	Internal test cohort (*n*=76)[a] (%)	External test cohort (*n*=393)[a] (%)	*p*-value[b]
Age				
≤60	59 (33)	27 (36)	67 (17)	<0.001
>60	119 (67)	49 (64)	326 (83)	
Gender				
F	102 (57)	42 (55)	219 (56)	0.928
M	76 (43)	34 (45)	174 (44)	
Smoking				
Never	28 (16)	12 (16)	41 (10)	0.137
Ever	150 (84)	64 (84)	352 (90)	
pT_stage				
T1 and T2	150 (84)	65 (86)	361 (92)	0.016
T3 and T4	28 (16)	11 (14)	32 (8.1)	
pN_stage				
N0 and N1	151 (85)	61 (80)	359 (91)	0.006
N2 and N3	27 (15)	15 (20)	34 (8.7)	
pM_stage				
M0	167 (94)	71 (93)	378 (96)	0.283
M1	11 (6.2)	5 (6.6)	15 (3.8)	
pTNM_stage				
I	98 (55)	40 (53)	254 (65)	0.134
II	39 (22)	18 (24)	67 (17)	
III and IV	41 (23)	18 (24)	72 (18)	
TIMM8B				
Low	91 (51)	36 (47)	196 (50)	0.860
High	87 (49)	40 (53)	197 (50)	

Notes: [a]data expressed as *n* (%); [b]Pearson's Chi-squared test or Fisher's exact test.
Abbreviations: pT: Pathological tumor; pN: Pathological node; pM: Pathological metastasis; pTNM: Pathological tumor-node-metastasis.

Th2 cells. The association between *TIMM8B* and immune checkpoint genes is depicted in Figure 6A, indicating a negative correlation with CD274, CTLA4, PDCD1, and TIGIT, which are potential targets for antitumor immunotherapy. Using the TIDE algorithm, we calculated the TIDE score for the TCGA LUAD cohort, revealing a significant positive correlation between *TIMM8B* levels and TIDE score (p=0.022) (Figure 6B). Kaplan–Meier analysis from the Kaplan–Meier plotter database further showed that the *TIMM8B*^{high} group had poorer OS compared to the *TIMM8B*^{low} group when treated with anti-PD1 immunotherapy (Figure 6C; HR = 1.44, p=0.009) or anti-CTLA4 immunotherapy (Figure 6D; HR = 1.88, p=0.055). These findings underscore *TIMM8B*'s role in shaping an immunosuppressive TME in LUAD, potentially fostering disease progression.

3.7. Interactions of *TIMM8B* with m6A RNA methylation and ferroptosis in LUAD

To investigate whether *TIMM8B* expression is influenced by m6A modification, we examined the relationship between *TIMM8B* and m6A-related genes in LUAD. In Figure 7A, the expression level of *TIMM8B* was found to be significantly correlated with 12 m6A-related genes, including *FTO* ($p=1.88\times10^{-3}$), *YTHDC2* ($p=3.00\times10^{-7}$), *METTL14* ($p=4.67\times10^{-2}$), *ZC3H13* ($p=5.63\times10^{-5}$), *YTHDC1* ($p=3.66\times10^{-4}$), *YTHDF1* ($p=4.75\times10^{-2}$), *YTHDF2* ($p=2.50\times10^{-3}$), *YTHDF3* ($p=3.60\times10^{-4}$), *WTAP* ($p=7.02\times10^{-7}$), *HNRNPC* ($p=1.43\times10^{-18}$), *RBMX* ($p=1.03\times10^{-3}$), and *IGF2BP1* ($p=2.33\times10^{-3}$). In addition, 17 out of 24 ferroptosis-related genes were significantly correlated with *TIMM8B* (Figure 7B): *SLC1A5* ($p=1.32\times10^{-6}$), *HSPA5* ($p=3.37\times10^{-2}$), *SLC7A11* ($p=3.27\times10^{-2}$), *CARS1* ($p=3.15\times10^{-4}$), *FANCD2* ($p=8.28\times10^{-3}$), *TFRC* ($p=3.1\times10^{-4}$), *MT1G* ($p=2.25\times10^{-7}$), *CISD1* ($p=1.78\times10^{-18}$), *ATP5MC3* ($p=4.13\times10^{-24}$), *HSPB1* ($p=1.22\times10^{-3}$), *GPX4* ($p=1.99\times10^{-8}$), *RPL8* ($p=8.74\times10^{-14}$), *DPP4* ($p=1.79\times10^{-3}$), *ALOX1* ($p=5.02\times10^{-3}$), *FDFT1* ($p=1.96\times10^{-3}$), *ACSL4* ($p=3.78\times10^{-2}$), and *NCOA4* ($p=3.01\times10^{-2}$). The GSEA analysis unveiled ferroptosis-related genes correlated with *TIMM8B* expression (Figure 7C). Comparison of high *TIMM8B* expression samples with low *TIMM8B* expression samples in the GSEA analysis indicated a significant difference in the enrichment of ferroptosis-marker and ferroptosis-suppressor genes. These findings suggest that *TIMM8B* is associated with m6A modification and ferroptosis in LUAD.

3.8. Interactions between *TIMM8B* and *TP53* mutations in LUAD

The somatic mutation rate of *TIMM8B* in TCGA LUAD is notably low at 0.2% (1/516), characterized by missense mutations, as illustrated in the Lollipop charts (Figure S5). This underscores the rarity of *TIMM8B* mutations in LUAD. A broader examination of the somatic mutation landscape in LUAD, using the TCGA cohort, reveals varying mutation frequencies across genes in the *TIMM8B*^{high} and *TIMM8B*^{low} subgroups. Notably, *TP53*, *TTN*, and *MUC16* emerge as the top three genes with the highest mutation frequencies (Figure 8A). Comparing the *TIMM8B*^{high} and *TIMM8B*^{low} groups in TCGA LUAD, we find no significant differences in the mutation profiles of *EGFR* (p=0.069) and *STK11* (p=1). However, the

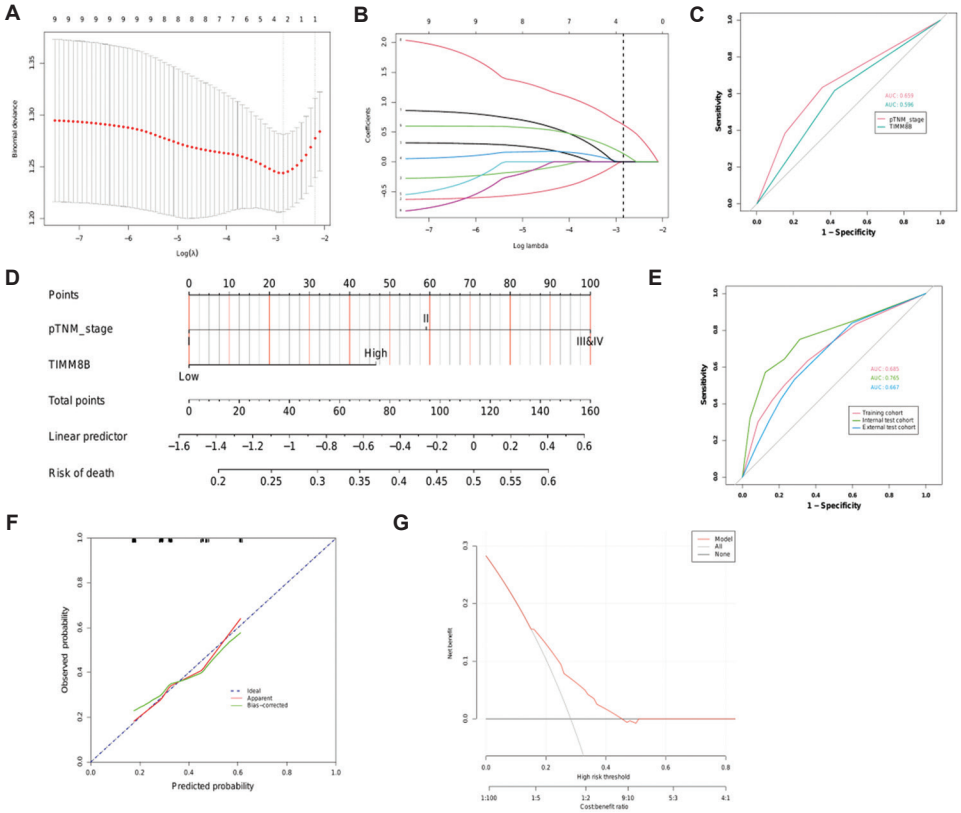

Figure 4. Development and validation of a nomogram incorporating *TIMM8B* for prognostic evaluation in LUAD. (A) Lasso regression cross-validation plot. (B) Lasso regression coefficient path plot. (C) ROC curve analysis of two candidate predictive indicators. (D) Nomogram prediction model containing *TIMM8B* for LUAD prognosis. (E) ROC curves of the nomogram prediction model. (F) Calibration curve of the nomogram prediction model for the training cohort. (G) Decision curve analysis of the nomogram for the training cohort.
Abbreviations: AUC: Area under the curve; *TIMM8B:* Translocase of inner mitochondrial membrane 8 homolog B; LUAD: Lung adenocarcinoma; ROC: Receiver operating characteristic.

TIMM8B^{high} group shows higher mutation rates in *KEAP1* (p=0.041), *KRAS* (p=0.004), and *TP53* (p=0.001) compared to the *TIMM8B*^{low} group (Figure 8B). Further analysis of the GSE72094 dataset also indicates a higher mutation rate of *TP53* (p=0.027) in the *TIMM8B*^{high} group, whereas the mutation rate of *EGFR* (p=0.029) is lower (Figure 8C). These findings strongly suggest a correlation between *TIMM8B* expression levels and *TP53* mutations in LUAD, highlighting potential implications for understanding disease progression and treatment response.

3.9. Dual roles of *TIMM8B* in chemotherapy resistance and small-molecule inhibitor sensitivity in LUAD

Analysis using the CTD database revealed that *TIMM8B* expression is downregulated by substances such as arsenite, arsenic, 1,2-dimethylhydrazine, and carbon tetrachloride, while being upregulated by known carcinogens such as vehicle emissions, tobacco smoke pollution, benzo(a)pyrene, ethanol, lead, and doxorubicin (Figure 9A). These findings suggest *TIMM8B*'s involvement in carcinogenic pathways induced by these agents. In addition, analysis of stemness features in the TCGA LUAD dataset indicated significantly elevated mRNAsi scores in *TIMM8B*^{high} subclusters (p=3.5 × 10^{-15}) (Figure 9B), implying a role for *TIMM8B* in promoting chemotherapy resistance. Furthermore, correlation analysis between *TIMM8B* expression levels and IC_{50} values of various drugs across multiple pathways consistently showed a negative correlation for inhibitors targeting CDK, PI3K/AKT/mTOR, AKT, mTOR, KSP, MAPK, HDAC, Survivin, IKK1/IKK2, BET, HSP90, and MEK1/2 pathways (Figure 9C). This suggests that higher *TIMM8B* expression may enhance sensitivity to these drugs. Conversely, a positive correlation was observed for common chemotherapeutic drugs, Cetuximab, BTK inhibitors, RPTK inhibitors, MDM2 inhibitors, GSK3 inhibitors, SRC inhibitors, TAK inhibitors, PKC inhibitors, and CHK inhibitors, indicating potential drug resistance associated with elevated *TIMM8B* expression. To assess the binding affinity of candidate drugs for *TIMM8B*, molecular

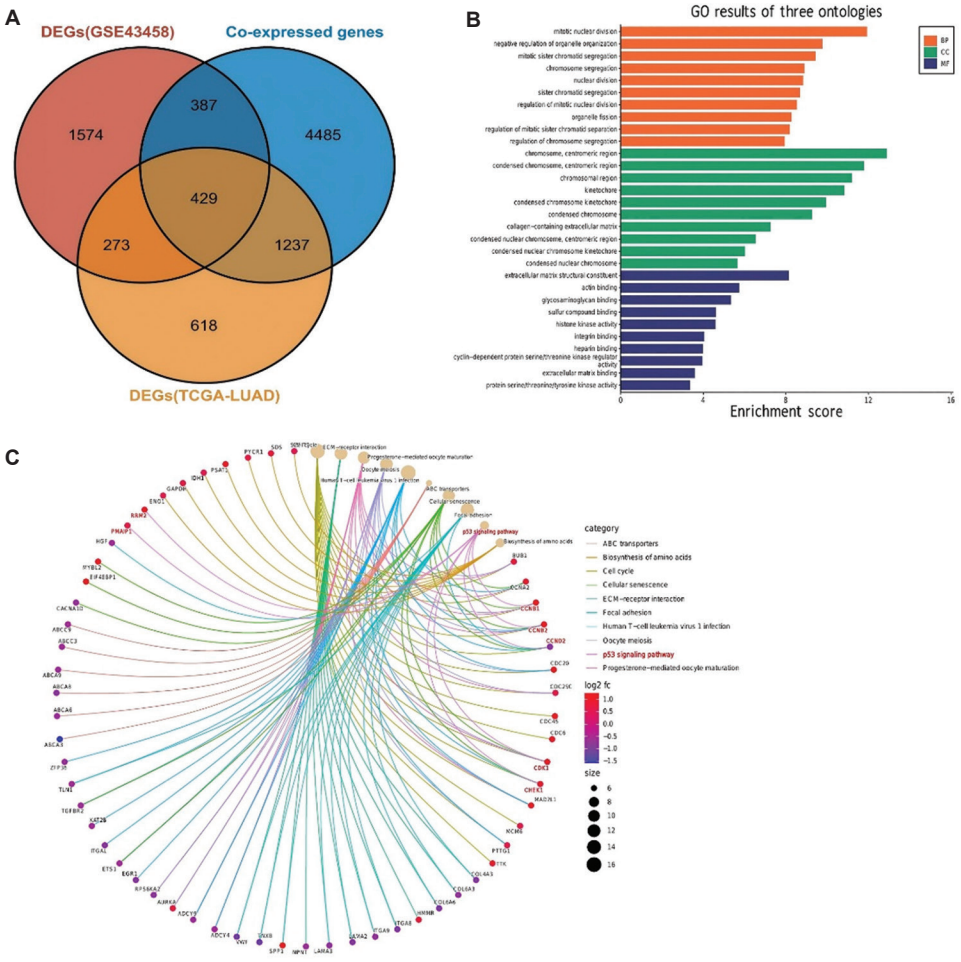

Figure 5. Analysis of *TIMM8B*-related genes in lung adenocarcinoma (LUAD) and enrichment analysis of intersecting genes. (A) A Venn diagram depicting the intersection of genes. (B) Bubble charts of BP, MF, and CC in GO analysis. (C) Pathway cnetplot of Kyoto Encyclopedia of Genes and Genomes pathway enrichment analysis of intersecting genes.
Abbreviations: DEG: Differentially expressed gene; *TIMM8B:* Translocase of inner mitochondrial membrane 8 homolog B; LUAD: Lung adenocarcinoma; BP: Biological process; MF: Molecular function; CC: Cellular component; GO: Gene ontology.

docking analysis using Autodock Vina v.1.2.2 revealed stable interactions and binding energies for Phenformin, PHA793887, WZ3105, and YM201636 (Figure S6). These results indicated visible hydrogen bonds and strong electrostatic interactions, with binding energies ranging from −5.4 to −7.9 kcal/mol, confirming robust binding stability. In summary, while *TIMM8B* overexpression in LUAD is associated with chemotherapy resistance to traditional drugs, it paradoxically enhances sensitivity to specific small molecule inhibitors targeting the PI3K/AKT/mTOR pathway. These insights underscore the dual role of *TIMM8B* in modulating LUAD pathophysiology and treatment responses, suggesting its potential as a therapeutic target in precision medicine approaches.

3.10. *TIMM8B* overexpression and prognostic significance in LUAD TMA samples

Our study demonstrates that the *TIMM8B* protein is significantly overexpressed in 80 LUAD samples compared to corresponding paracancerous tissues from LUAD TMA samples (Figure 10A-C). To validate the association between *TIMM8B* protein expression and clinicopathological features in LUAD TMA samples, we conducted a Mann–Whitney *U* test using the TCGA TMA samples, dividing them into $TIMM8B^{high}$ and $TIMM8B^{low}$ groups. Table 3 reveals a significant difference in *TIMM8B* expression levels based on pTNM stage (p=0.007). However, no significant correlations were found between *TIMM8B* expression and age (p=0.700), gender (p=0.612), histological grade (p=0.814), pT stage (p=0.709), pN stage

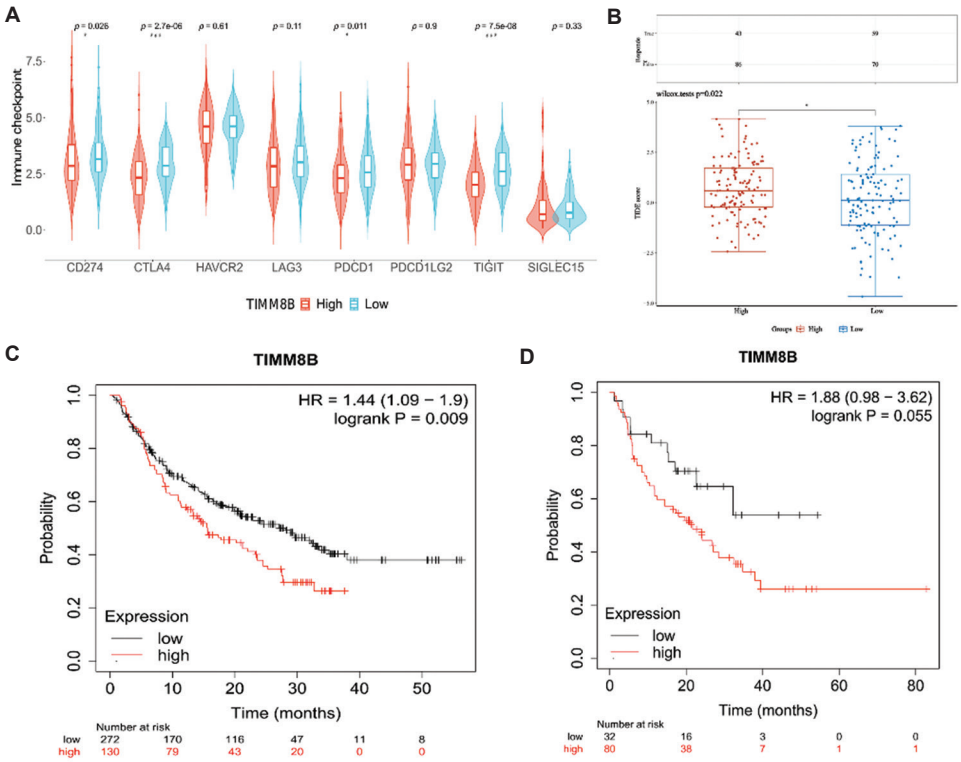

Figure 6. Immune checkpoint-related gene expression analysis in lung adenocarcinoma (LUAD). (A) Expression distribution of immune checkpoint genes in translocase of inner mitochondrial membrane 8 homolog B (*TIMM8B*)^{low} and *TIMM8B*^{high} groups of the Cancer Genome Atlas LUAD. The x-axis represents sample groups, and the y-axis represents gene expression distribution. Different colors indicate different groups. (B) Statistical comparison of immune response scores between groups using the Wilcox test. (C) *TIMM8B* expression and anti-PD-1 treatment survival analysis using messenger RNA (mRNA) RNA-seq data from the Kaplan–Meier plotter (n = 402). (D) *TIMM8B* expression and anti-cytotoxic T-lymphocyte associated protein 4 treatment survival analysis using mRNA RNA-seq data from the Kaplan–Meier plotter (n = 112).

(p=0.710), and pM stage (p=0.057). These findings suggest that *TIMM8B* expression is associated specifically with TNM stage, highlighting its potential as a biomarker for poor prognosis in LUAD, consistent with the *TIMM8B* mRNA findings in TCGA LUAD. Kaplan–Meier analysis performed on LUAD TMA samples indicated a negative correlation between *TIMM8B* expression and OS of LUAD patients (p=0.027), as illustrated in Figure 10D. To further explore the independent prognostic value of *TIMM8B* in LUAD, we conducted univariate and multivariate Cox proportional analyses using the TCGA TMA samples. The forest plot in Figure 10E presents the results of the univariate Cox proportional analysis, showing that histological grade, pN stage, pM stage, pTNM stage, and *TIMM8B* expression significantly influence OS in LUAD. Moreover, the multivariate Cox proportional analysis confirmed that histological grade, pN stage, and pM stage are independent prognostic factors for OS. In summary, our findings underscore *TIMM8B* as a predictor of poor prognosis in LUAD, emphasizing its potential clinical relevance in prognostic stratification and therapeutic decision-making.

3.11. Effects of *TIMM8B* knockdown on PD-L1 expression and G1 phase arrest

In our further investigation, *TIMM8B*, TP53, PD-L1, and EGFR expression levels were assessed in five LUAD cell lines (Figure 11A). *TIMM8B* was found to be overexpressed in the H1299 cell line, prompting the design of a siRNA to target *TIMM8B* in these cells. The efficiency of *TIMM8B* knockdown is depicted in Figure 11B, demonstrating effective reduction of *TIMM8B* expression. Subsequent analysis revealed that silencing *TIMM8B* significantly increased EGFR expression and decreased PD-L1 expression (Figure 11C). To investigate the functional role of *TIMM8B* in LUAD, cell models with *TIMM8B* shRNA and control groups were established using the H1299 cell line. The knockdown efficiency is illustrated in Figures 11D-F, confirming effective reduction of *TIMM8B* expression in the shRNA-treated cells compared to controls. Importantly, *TIMM8B* knockdown induced notable G1 phase arrest in the cell cycle (Figures 11G-I), suggesting a potential role of *TIMM8B* in cell cycle regulation in LUAD. These findings contribute to

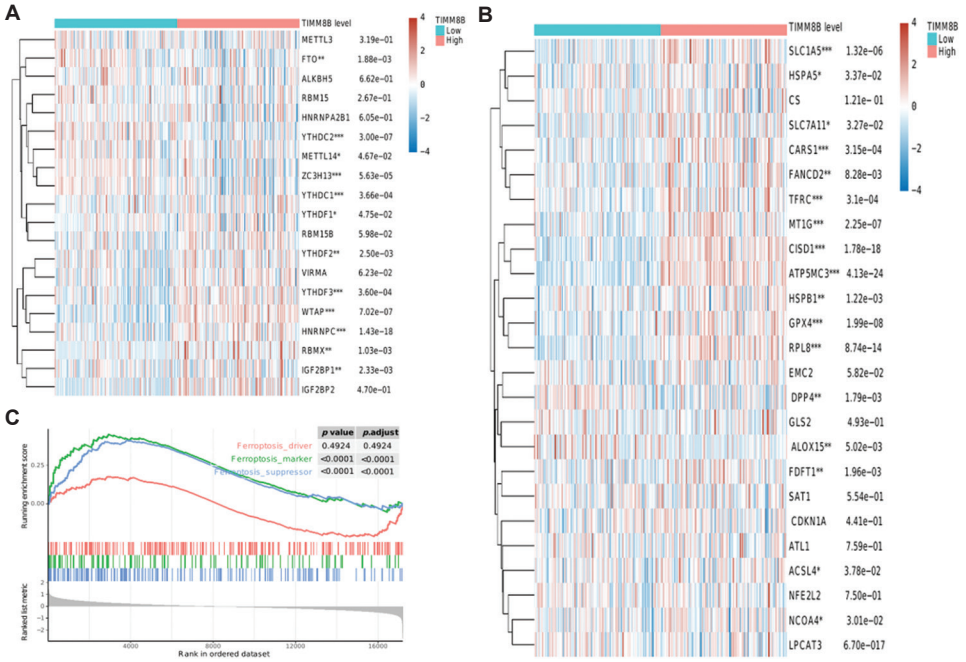

Figure 7. Correlation analysis between translocase of inner mitochondrial membrane 8 homolog B (*TIMM8B*) expression and m6A- and ferroptosis-related genes in lung adenocarcinoma. (A) Heatmap of Spearman coefficients for m6A-related genes. (B) Heatmap of Spearman coefficients for ferroptosis-related genes. (C) Gene set enrichment analysis of ferroptosis-related genes associated with *TIMM8B* expression, showing significant differences in the enrichment of ferroptosis-marker and ferroptosis-suppressor genes between high and low *TIMM8B* expression samples.

understanding the biological significance of *TIMM8B* in LUAD and its potential as a therapeutic target.

3.12. Inflammatory response induced by *TIMM8B* knockdown via *CCL2*

To explore the downstream target genes and signaling pathways influenced by *TIMM8B*, we established cell models with *TIMM8B* shRNA and control groups using the H1299 cell line, followed by transcriptomic RNA sequencing. The volcano plot illustrates differential expression, with 251 genes upregulated and 86 genes downregulated upon *TIMM8B* knockdown compared to controls (Figure 12A). These findings are further highlighted in the heatmap, showing distinct clustering of DEGs between the two groups (Figure 12C). KEGG pathway enrichment analysis reveals that DEGs between *TIMM8B* knockdown and control groups are primarily associated with substance metabolism, energy metabolism, insulin resistance, transcriptional inactivation, ECM–receptor interaction, and the PI3K–AKT signaling pathway (Figure 12B). GO enrichment analysis indicates that DEGs are enriched in cellular processes, biological regulation, and metabolic processes within the biological process category. Enrichment in cellular components includes protein complexes, whereas molecular function enrichment involves binding, catalytic activity, and transcription regulatory activity (Figure 12D). GSEA shows enrichment in inflammation response, interferon-gamma response, and tumor necrosis factor alpha (TNF-α) signaling via nuclear factor kappa B (NF-κB) pathways upon *TIMM8B* knockdown (Figure 12E). The standardized enrichment scores highlight statistically significant differences in pathways such as E2F targets, inflammation response, and interferon-gamma response (Figure 12F). Utilizing Cytoscape for protein–protein interaction network analysis of DEGs identifies hub genes, including *CXCL8*, *CCL2*, and *PXDN* (Figure 12G). Specifically, *TIMM8B* knockdown significantly decreases *CCL2* expression (Figure 12H), suggesting *CCL2* as a downstream target gene influenced by *TIMM8B*. Overall, these results indicate that downregulation of *TIMM8B* activates inflammatory signaling pathways, with *CCL2* identified as a key hub gene modulated by *TIMM8B*.

4. Discussion

In this study, *TIMM8B* is overexpressed in multiple cancers and is correlated with poorer OS in LUAD. *TIMM8B*-related gene analyses suggest roles in various cellular processes. *TIMM8B* shapes an immunosuppressive TME in LUAD. Elevated *TIMM8B* expression is associated with TP53 mutations and chemotherapy resistance. Knockdown of *TIMM8B* in H1299 cells induces G1 phase arrest, highlighting its role in cell cycle regulation. In addition,

Figure 8. Insights from translocase of inner mitochondrial membrane 8 homolog B (*TIMM8B*) mutation analysis in the Cancer Genome Atlas (TCGA) lung adenocarcinoma (LUAD). (A) Oncoplot of the somatic landscape in the TCGA LUAD tumor cohort (n = 516). (B) Comparative analysis of *EGFR*, *KEAP1*, *KRAS*, *STK11*, and *TP53* messenger RNA mutation profiles between *TIMM8B*^{high} and *TIMM8B*^{low} groups in TCGA LUAD. (C) Comparative analysis of *EGFR*, *KRAS*, *STK11*, and *TP53* mutation profiles between *TIMM8B*^{high} and *TIMM8B*^{low} groups using clinical data from GSE72094.

knockdown of *TIMM8B* downregulates PD-L1 and *CCL2*-mediated immune and inflammatory responses.

In our study, *TIMM8B* mRNA is significantly overexpressed in 15 of 33 cancer types, including LUAD, compared to normal tissues. This elevated expression in LUAD is validated by multiple datasets, including TCGA, GTEx, and GEO (GSE10072, GSE31210), as well as protein expression in LUAD TMA, indicating its potential involvement in LUAD pathogenesis. According to Del Puerto-Nevado L's study,[17] the *TIMM8B* protein is elevated in both tumor and mucosal tissues in diabetic patients. Notably, differential expression of *TIMM8B* in the colonic mucosa of people with diabetes versus non-diabetic individuals was confirmed. Furthermore, normal colon epithelial cells exposed to high-glucose conditions exhibited increased *TIMM8B* levels. These findings suggest that T2DM induces specific *TIMM8B* alterations in the normal mucosa of colorectal cancer patients, supporting the idea of a carcinogenic field effect in a diabetic environment. Prognostically, high *TIMM8B* levels are associated with poor outcomes in ACC, LIHC, UVM, and LUAD. In contrast, elevated *TIMM8B* expression correlates with improved survival in ovarian cancer (OV). Wang's study supports this by incorporating *TIMM8B* into a prognostic model for OV based on cuproptosis-related genes.[24] These observations suggest that the effects of *TIMM8B* in diverse tumors are multifaceted and may be influenced by the TME of different cancers. In this study, specifically for LUAD, increased *TIMM8B* consistently predicts worse survival across various cohorts (GEPIA2, Kaplan–Meier Plotter, TCGA, GSE72094), with protein expression also confirmed in LUAD TMA. Clinically, high *TIMM8B* levels in LUAD are associated with advanced tumor stages (pT, pN, and pTNM), older age, and serve as an independent prognostic factor (TCGA and GSE72094). A validated nomogram integrating *TIMM8B* expression and pTNM stages demonstrates robust predictive performance for LUAD prognosis. Furthermore, elevated *TIMM8B* protein levels in LUAD TMA are linked to advanced pTNM stages and poor OS, underscoring its

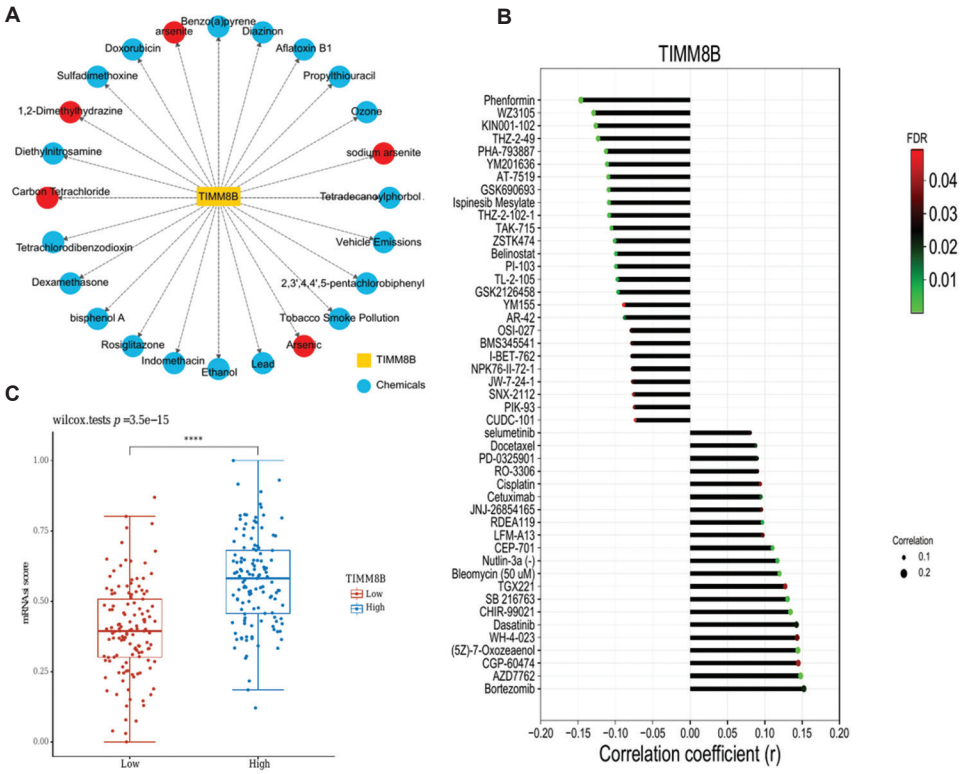

Figure 9. Correlation analysis of translocase of inner mitochondrial membrane 8 homolog B (*TIMM8B*) and drug sensitivity in lung adenocarcinoma (LUAD). (A) Prediction of chemicals influencing *TIMM8B* via the Comparative Toxicogenomics Database. Red denotes chemicals inhibiting *TIMM8B* expression, whereas blue signifies those enhancing *TIMM8B* expression. (B) messenger RNA stemness index (mRNAsi) scores for *TIMM8B* Low and High subclusters in the Cancer Genome Atlas LUAD dataset. Elevated mRNAsi indicates chemotherapy resistance. (C) Correlation between drug sensitivity and *TIMM8B* messenger RNA expression using the GDSC database. The lollipop plot illustrates Spearman's correlation coefficient (false discovery rate ≥ 0.05).

independent prognostic value. Collectively, these findings highlight *TIMM8B*'s critical role in cancer progression and its potential as a prognostic biomarker.

A comprehensive analysis of *TIMM8B*'s co-expressed and DEGs reveals its significant involvement in LUAD. *TIMM8B* is involved in regulating cell cycle progression, mitosis, and cellular adhesion, suggesting its potential role in LUAD pathogenesis. Knockdown studies demonstrating G1/S phase arrest in LUAD cells confirm *TIMM8B*'s impact on cell cycle regulation. Similarly, TIMM17A knockdown led to a decreased proportion of cells in the S phase, suggesting that TIMM17A promotes cellular proliferation.[9] In contrast, inhibition of TIMM44 induced G1/S phase arrest in bladder cancer cells.[25] Further analysis using *TIMM8B* shRNA in the H1299 cell model demonstrates that *TIMM8B* influences cellular functions such as metabolism and interactions with the ECM. Moreover, GSEA analysis reveals E2F target signaling is enriched in *TIMM8B* knockdown cells. Among these E2F target genes, many encode essential cell cycle regulators.[26] These findings suggest that *TIMM8B* participates in various cellular processes from fundamental basis to tumor biology, potentially contributing to the aggressive behavior and adaptability of LUAD cells. TP53, a crucial tumor suppressor gene, is involved in DNA repair, apoptosis, and cell cycle control. Mutations in TP53 often result in the loss of its tumor-suppressive functions, leading to genomic instability and cancer progression.[27] The association between high *TIMM8B* expression and increased TP53 mutation rates implies that *TIMM8B* may interact with pathways regulated by TP53, thus contributing to tumor progression by impacting these critical cellular processes. *TIMM8B* is also linked to m6A RNA methylation and ferroptosis-related genes, suggesting it may modulate RNA stability and translational efficiency through m6A modifications and influence ferroptosis. These roles implicate *TIMM8B* in maintaining genetic stability and managing oxidative stress, further underscoring its involvement in LUAD pathogenesis. Elevated analysis using the CTD datasets indicates that carcinogens such as vehicle emissions, tobacco smoke pollution, benzo(a) pyrene, ethanol, and lead upregulate *TIMM8B* expression. It suggests *TIMM8B*'s involvement in the carcinogenic pathways activated by these agents, potentially contributing

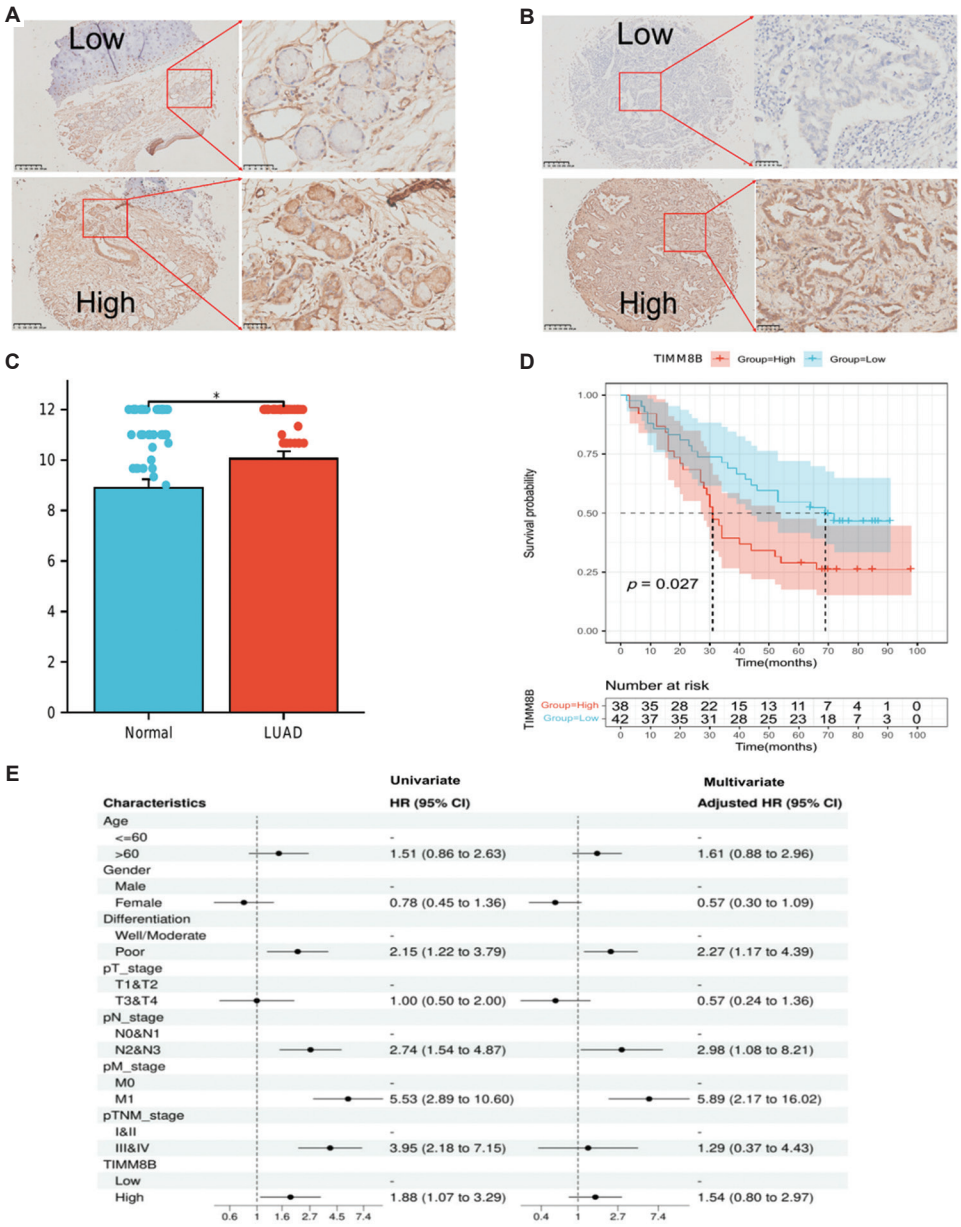

Figure 10. Translocase of inner mitochondrial membrane 8 homolog B (*TIMM8B*) is overexpressed and predictive of poor prognosis for lung adenocarcinoma (LUAD) tissue microarray samples. (A) Representative images of *TIMM8B* immunohistochemical (IHC) staining in adjacent tissues. Scale bars: 100 μm; magnification: ×40. (B) Representative images of *TIMM8B* IHC staining in LUAD tissues. Scale bars: 100 μm; magnification: ×40. (C) Protein expression levels of *TIMM8B* in human LUAD (n = 80) were significantly higher than those in corresponding paracancerous tissues (n = 79). (D) Kaplan–Meier analysis showed that LUAD patients with high *TIMM8B* expression had shortened overall survival. (E) Univariate and multivariate Cox model analyses illustrating the prognostic significance of *TIMM8B* expression in LUAD (*p<0.05).
Abbreviations: CI: Confidence interval; HR: Hazard ratio.

to LUAD development. Stemness feature analysis using the mRNAsi score from the TCGA LUAD dataset reveals that elevated *TIMM8B* levels may enhance stemness characteristics in cancer cells, contributing to chemotherapy resistance. Moreover, data from the GDCA datasets show a positive correlation between *TIMM8B* expression and resistance to conventional chemotherapeutic drugs such as docetaxel, cisplatin, and bleomycin. Interestingly, despite its role in chemotherapy resistance, elevated *TIMM8B* levels in LUAD are linked to increased sensitivity to certain small molecule inhibitors, particularly those targeting the PI3K/AKT/mTOR pathway and cyclin-dependent kinases

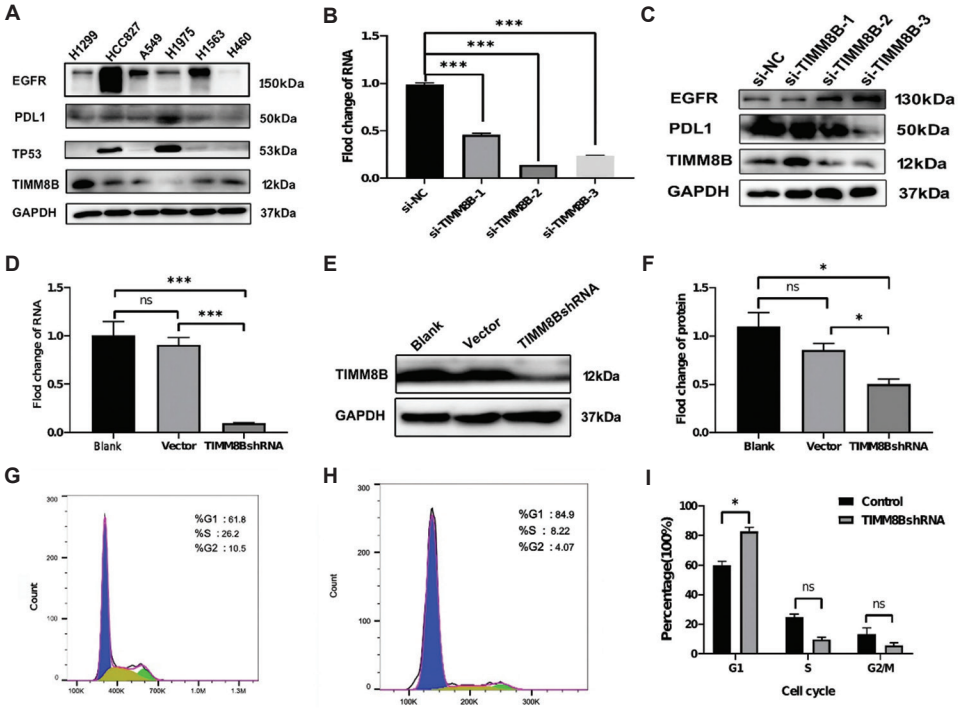

Figure 11. Knockdown of translocase of inner mitochondrial membrane 8 homolog B (*TIMM8B*) regulates PD-L1 expression and induces G1 phase arrest in lung adenocarcinoma (LUAD) H1299 cells. (A) Protein levels of EGFR, PDL1, TP53, and *TIMM8B* were analyzed via western blot in LUAD cell lines. (B) Measurement of *TIMM8B* RNA levels in H1299 cells subjected to si-*TIMM8B* knockdown. (C) Detection of EGFR, PDL1, and *TIMM8B* protein levels in H1299 cells treated with si-NC and si-*TIMM8B*. (D-F) Analysis of *TIMM8B* RNA and protein levels in stable *TIMM8B* knockdown H1299 cells normalized to GAPDH expression. (G-I) Assessment of cell cycle progression in H1299/Vector and H1299/*TIMM8B*-shRNA cells using flow cytometry assays. The bar chart illustrates the distribution of cells in G1, S, or G2/M phase.
Notes: ns: $p>0.05$; *$p<0.05$; **$p<0.01$; ***$p<0.001$.

(CDKs). This finding suggests that while *TIMM8B* confers resistance to traditional chemotherapies, it may also represent a potential vulnerability that can be exploited with targeted therapies.

Our findings underscore the pivotal role of *TIMM8B* in cancer immunity, particularly in LUAD. XCELL database analysis reveals that high *TIMM8B* levels in LUAD are associated with reduced immune cell infiltration levels, particularly CD8+ and CD4+ T cells, and an increased presence of CD4+ Th2 cells. Studies indicate that CD8+ T cells are crucial in antitumor immunity, directly killing tumor cells and boosting immune responses, whereas CD4+ T cells support this function through cytokine release.[28] However, CD4+ Th2 cells in tumor immunotherapy suppress antitumor immunity, contribute to an immunosuppressive TME, and may reduce the efficacy of immune checkpoint inhibitors.[29] Furthermore, *TIMM8B* showed a negative correlation with the stroma score, microenvironment score, and immune score, suggesting that *TIMM8B* may contribute to an immune desert-like TME, potentially leading to poor responses to immunotherapy.[30] Moreover, *TIMM8B* negatively correlates with immune checkpoint genes (*CD274, CTLA4, PDCD1,* and *TIGIT*), suggesting that its overexpression may hinder effective immunotherapy responses. TIDE score analysis indicates that higher *TIMM8B* levels are linked to a higher TIDE score, reflecting poorer responses to immunotherapy.[18] Kaplan–Meier Plotter data further confirm that LUAD patients with high *TIMM8B* expression have worse OS when treated with anti-PD1 or anti-CTLA4 therapies. Collectively, these findings suggest that *TIMM8B* contributes to an immunosuppressive TME in LUAD, influences cancer immunity, and may serve as a potential biomarker for LUAD immunotherapy. Transcriptomic analysis indicates that reduced *TIMM8B* levels activate inflammatory pathways, including the interferon-gamma response and TNF-α signaling through the NF-κB pathway. These pathways are essential for mediating immune reactions and maintaining cellular inflammatory states.[31,32] A significant outcome of *TIMM8B* silencing is the substantial reduction in *CCL2* and *PDL1* expression. *CCL2* is essential for recruiting immune cells to sites of inflammation and has been associated with tumor progression by promoting a pro-tumorigenic

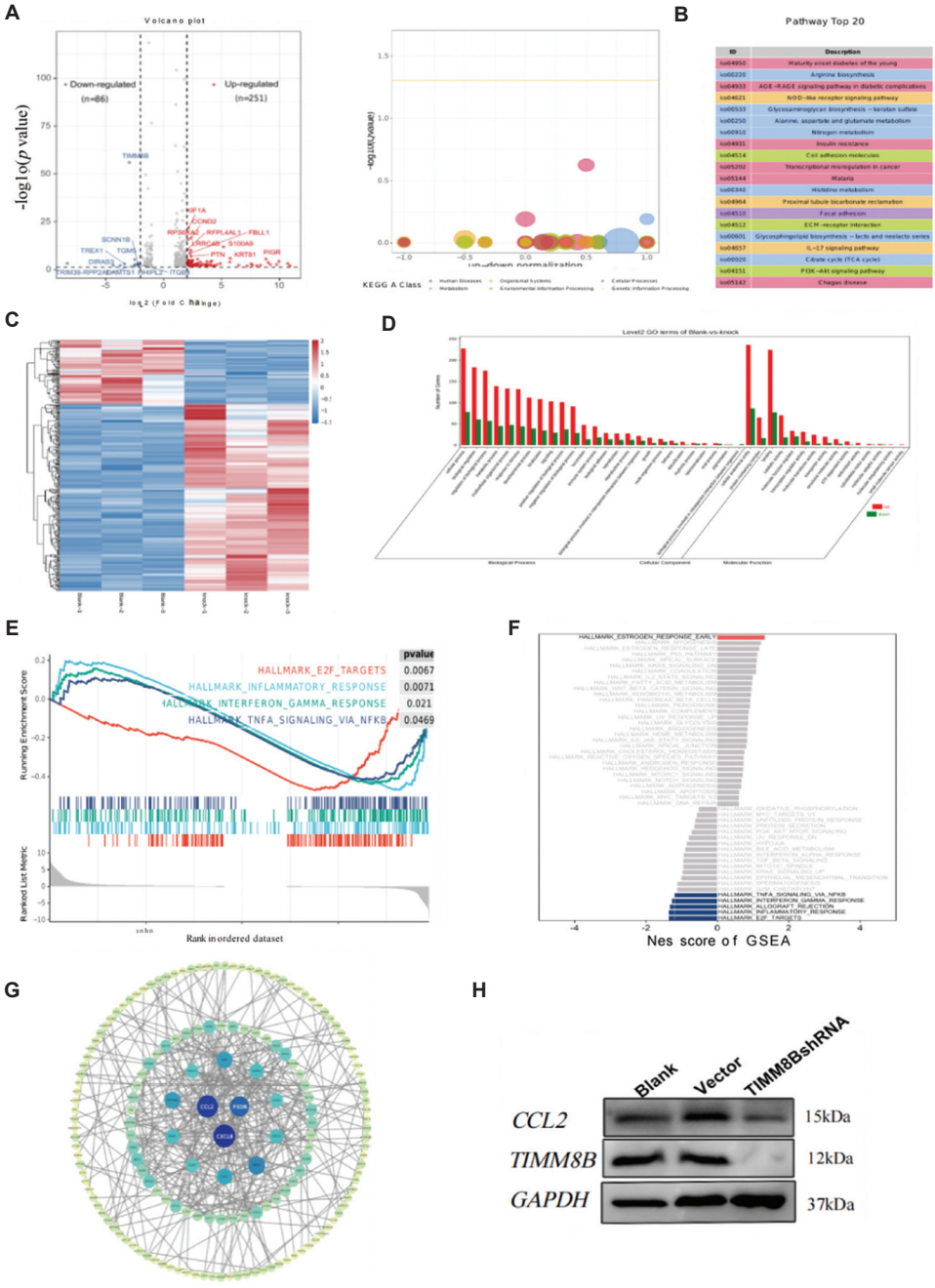

Figure 12. Analysis of translocase of inner mitochondrial membrane 8 homolog B (*TIMM8B*) regulated pathways in lung adenocarcinoma. (A) Volcano plot comparing up- and down-regulated genes between H1299/*TIMM8B* Small hairpin RNAs (shRNA) and H1299/vector. (B) Kyoto Encyclopedia of Genes and Genomes enrichment bubble diagram illustrating differentially expressed genes (DEGs). (C) Heatmap comparing DEGs between H1299/*TIMM8B* shRNA and H1299/vector. (D) Bar plot visualization of gene ontology term analysis for biological process, molecular function, and cellular component of DEGs. (E) Representative enriched pathways based on HALLMARK terms, including inflammatory response pathway, interferon gamma response pathway, and tumor necrosis factor alpha signaling via nuclear factor kappa B. (F) Bar graphs displaying results of Gene Set Enrichment Analysis. All cascades, except gray, showed significant enrichment ($p<0.05$). (G) Construction of the regulatory network of *TIMM8B* using DEGs in Cytoscape. (H) Detection of *CCL2* and *TIMM8B* protein levels in H1299 cells treated with *TIMM8B* shRNA.

environment.[33] Similarly, PDL1 is crucial for tumor immune evasion by binding to the *PD-1* receptor on T cells, inhibiting their activity.[28] The reduced expression of these molecules following *TIMM8B* knockdown suggests that *TIMM8B* plays a crucial role in sustaining their expression, thereby maintaining the inflammatory and

Table 3. Patient demographics and baseline characteristics from lung adenocarcinoma tissue microarray samples

Characteristic	*TIMM8B*		*p*-value[b]
	Low (*n*=42)[a] (%)	High (*n*=38)[a] (%)	
Age			
≤60	25 (60)	21 (55)	0.700
>60	17 (40)	17 (45)	
Gender			
Female	20 (48)	19 (50)	0.832
Male	22 (52)	19 (50)	
Histological grade			
Well/Moderate	21 (50)	20 (53)	0.814
Poor	21 (50)	18 (47)	
pT_stage			
T1 and T2	33 (79)	27 (75)	0.709
T3 and T4	9 (21)	9 (25)	
pN_stage			
N0 and N1	30 (71)	25 (68)	0.710
N2 and N3	12 (29)	12 (32)	
pM_stage			
M0	37 (88)	27 (71)	0.057
M1	5 (12)	11 (29)	
pTNM_stage			
I and II	27 (64)	13 (34)	0.007
III and IV	15 (36)	25 (66)	

Notes: [a]data expressed as *n* (%); [b]Pearson's Chi-squared test or Fisher's exact test.
Abbreviations: pT: Pathological tumor; pN: Pathological node; pM: Pathological metastasis; pTNM: Pathological tumor-node-metastasis.

immune-suppressive environment in tumors. *TIMM8B* modulation might reduce the tumor's capacity to evade the immune system and lessen inflammation-mediated tumorigenic processes. Therefore, inhibiting *TIMM8B* could disrupt tumor-promoting signaling pathways and enhance antitumor immunity.

However, our study still has some limitations. Our findings suggest that *TIMM8B* is involved in the infiltration of immune cells in LUAD, but the mechanism is unclear and requires further investigation.

5. Conclusion

Our extensive study of *TIMM8B* in LUAD reveals its diverse roles in cancer progression. These findings not only enhance our understanding of LUAD pathogenesis but also pave the way for future research aiming to leverage *TIMM8B* as a therapeutic target and biomarker in clinical oncology.

Acknowledgments

We extend our gratitude to Bioinformatics (https://www.bioinformatics.com.cn), Home for Researchers (https://www.home-for-researchers.com/), Hiplot (https://hiplot.com.cn), and MSTATA (https://app1.mstata.com/app/freetrial) for their invaluable support in data analysis and visualization.

Funding

This work was supported by the Science and Technology Project Grant of Zhuhai (grant number: 2220004000224).

Conflict of interest

The authors declare no competing interests.

Author contributions

Conceptualization: Zhihui Wang, Beilong Zhong
Data curation: Zhuli Zheng, Libao Gong, Hongcheng Zhong
Formal analysis: Zhuli Zheng
Investigation: Zhuli Zheng, Yunyan Cong
Methodology: Bingjiang Huang
Writing–original draft: Zhuli Zheng
Writing–review & editing: Zhihui Wang

Ethics approval and consent to participate

The study was conducted with the approval of the Ethics Committee of The Fifth Affiliated Hospital of Sun Yat-sen University, in accordance with the Declaration of Helsinki. Informed consent was obtained from all participants.

Consent for publication

Not applicable.

Availability of data

The TCGA dataset via the GDC portal (https://portal.gdc.cancer.gov). The GTEx dataset was sourced from the GTEx portal (https://www.gtexportal.org/home/datasets). GSE31210、 GSE10072, and GSE72094 were downloaded in MINiML format from the GEO database (http://ncbi.nlm.nih.gov/geo/).GEPIA2 online database (http://gepia2.cancer-pku.cn/).The Kaplan–Meier plotter database (http://kmplot.com/analysis/). Ferroptosis-related genes were available in the FerrDb database (http://www.zhounan.org/ferrdb/current/).To explore potential therapeutic implications of *TIMM8B* in LUAD, we examined its correlation with drug responses using IC_{50} data obtained from the GDSC database (https://www.cancerrxgene.org/). To predict potential associations between *TIMM8B* and chemicals, we utilized the Comparative Toxicogenomics

Database (CTD) (https://ctdbase.org/). For viewing molecular structures of relevant drugs, the PubChem database (https://pubchem.ncbi.nlm.nih.gov/).*TIMM8B*'s 3D coordinates were obtained from the Protein Data Bank (PDB) (http://www.rcsb.org/pdb/home/home.do).

References

1. Bray F, Laversanne M, Sung H, *et al*. Global cancer statistics 2022: GLOBOCAN estimates of incidence and mortality worldwide for 36 cancers in 185 countries. *CA Cancer J Clin*. 2024;74(3):229-263.

   doi: 10.3322/caac.21834

2. Suster DI, Mino-Kenudson M. Molecular pathology of primary non-small cell lung cancer. *Arch Med Res*. 2020;51(8):784-798.

   doi: 10.1016/j.arcmed.2020.08.004

3. Thai AA, Solomon BJ, Sequist LV, Gainor JF, Heist RS. Lung cancer. *Lancet*. 2021;398(10299):535-554.

   doi: 10.1016/S0140-6736(21)00312-3

4. Chen VW, Ruiz BA, Hsieh MC, Wu XC, Ries LAG, Lewis DR. Analysis of stage and clinical/prognostic factors for lung cancer from SEER registries: AJCC staging and collaborative stage data collection system. *Cancer*. 2014;120 Suppl 23:3781-3792.

   doi: 10.1002/cncr.29045

5. Chiu HY, Tay EXY, Ong DST, Taneja R. Mitochondrial dysfunction at the center of cancer therapy. *Antioxid Redox Signal*. 2020;32(5):309-330.

   doi: 10.1089/ars.2019.7898

6. Bauer MF, Hofmann S, Neupert W, Brunner M. Protein translocation into mitochondria: The role of TIM complexes. *Trends Cell Biol*. 2000;10(1):25-31.

   doi: 10.1016/s0962-8924(99)01684-0

7. Pfanner N, Warscheid B, Wiedemann N. Mitochondrial proteins: From biogenesis to functional networks. *Nat Rev Mol Cell Biol*. 2019;20(5):267-284.

   doi: 10.1038/s41580-018-0092-0

8. Salhab M, Patani N, Jiang W, Mokbel K. High TIMM17A expression is associated with adverse pathological and clinical outcomes in human breast cancer. *Breast Cancer*. 2012;19(2):153-160.

   doi: 10.1007/s12282-010-0228-3

9. Cai J, Chen J, Huang L, *et al.* A TIMM17A regulatory network contributing to breast cancer. *Front Genet*. 2021;12:658154.

   doi: 10.3389/fgene.2021.658154

10. Zhang Y, Lin L, Wu Y, Bing P, Zhou J, Yu W. Upregulation of TIMM8A is correlated with prognosis and immune regulation in BC. *Front Oncol*. 2022;12:922178.

    doi: 10.3389/fonc.2022.922178

11. Wang Z, Li S, Xu F, *et al*. ncRNAs-mediated high expression of TIMM8A correlates with poor prognosis and act as an oncogene in breast cancer. *Cancer Cell Int*. 2022;22(1):177.

    doi: 10.1186/s12935-022-02595-x

12. Zhu X, Yuan Z, Cheng S, *et al*. TIMM8A is associated with dysfunction of immune cell in BRCA and UCEC for predicting anti-PD-L1 therapy efficacy. *World J Surg Oncol*. 2022;20(1):336.

    doi: 10.1186/s12957-022-02736-6

13. Jin H, Kendall E, Freeman TC, Roberts RG, Vetrie DL. The human family of Deafness/Dystonia peptide (DDP) related mitochondrial import proteins. *Genomics*. 1999;61(3):259-267.

    doi: 10.1006/geno.1999.5966

14. Badenhop RF, Cherian S, Lord RS, Baysal BE, Taschner PE, Schofield PR. Novel mutations in the SDHD gene in pedigrees with familial carotid body paraganglioma and sensorineural hearing loss. *Genes Chromosomes Cancer*. 2001;31(3):255-263.

    doi: 10.1002/gcc.1142

15. Hoekstra AS, van den Ende B, Julia XP, *et al*. Simple and rapid characterization of novel large germline deletions in SDHB, SDHC and SDHD-related paraganglioma. *Clin Genet*. 2017;91(4):536-544.

    doi: 10.1111/cge.12843

16. Zhang J, Zhou X, Zhu C, *et al.* Wholegenome identification and systematic analysis of lncRNAmRNA coexpression profiles in patients with cutaneous basal cell carcinoma. *Mol Med Rep.* 2021;24(3):631.

    doi: 10.3892/mmr.2021.12270

17. Del Puerto-Nevado L, Santiago-Hernandez A, Solanes-Casado S, *et al.* Diabetes-mediated promotion of colon mucosa carcinogenesis is associated with mitochondrial dysfunction. *Mol Oncol*. 2019;13(9):1887-1897.

    doi: 10.1002/1878-0261.12531

18. Jiang P, Gu S, Pan D, *et al.* Signatures of T cell dysfunction and exclusion predict cancer immunotherapy response. *Nat Med*. 2018;24(10):1550-1558.

    doi: 10.1038/s41591-018-0136-1

19. Li Y, Xiao J, Bai J, *et al.* Molecular characterization and clinical relevance of m(6)A regulators across 33 cancer types. *Mol Cancer*. 2019;18(1):137.

    doi: 10.1186/s12943-019-1066-3

20. Liu Z, Zhao Q, Zuo ZX, *et al.* Systematic analysis of the aberrances and functional implications of ferroptosis in cancer. *iScience*. 2020;23(7):101302.

    doi: 10.1016/j.isci.2020.101302

21. Malta TM, Sokolov A, Gentles AJ, *et al*. Machine learning identifies stemness features associated with oncogenic dedifferentiation. *Cell*. 2018;173(2):338-354.e15.

doi: 10.1016/j.cell.2018.03.034

22. Morris GM, Huey R, Olson AJ. Using AutoDock for ligand-receptor docking. *Curr Protoc Bioinformatics*. 2008;Chapter 8:Unit 8 14.

doi: 10.1002/0471250953.bi0814s24

23. Wang Y, Bryant SH, Cheng T, *et al*. PubChem BioAssay: 2017 update. *Nucleic Acids Res*. 2017;45(D1):D955-D963.

doi: 10.1093/nar/gkw1118

24. Wang K, Zhang Y, Ao M, Luo H, Mao W, Li B. Multi-omics analysis defines a cuproptosis-related prognostic model for ovarian cancer: Implication of WASF2 in cuproptosis resistance. *Life Sci*. 2023;332:122081.

doi: 10.1016/j.lfs.2023.122081

25. Zhang L, Shi X, Zhang L, Mi Y, Zuo L, Gao S. A first-in-class TIMM44 blocker inhibits bladder cancer cell growth. *Cell Death Dis*. 2024;15(3):204.

doi: 10.1038/s41419-024-06585-x

26. Engeland K. Cell cycle regulation: p53-p21-RB signaling. *Cell Death Differ*. 2022;29(5):946-960.

doi: 10.1038/s41418-022-00988-z

27. Voskarides K, Giannopoulou N. The role of TP53 in adaptation and evolution. *Cells*. 2023;12(3):512.

doi: 10.3390/cells12030512

28. Chen L, Flies DB. Molecular mechanisms of T cell co-stimulation and co-inhibition. *Nat Rev Immunol*. 2013;13(4):227-242.

doi: 10.1038/nri3405

29. Speiser DE, Chijioke O, Schaeuble K, Munz C. CD4(+) T cells in cancer. *Nat Cancer*. 2023;4(3):317-329.

doi: 10.1038/s43018-023-00521-2

30. Park S, Ock CY, Kim H, *et al*. Artificial intelligence-powered spatial analysis of tumor-infiltrating lymphocytes as complementary biomarker for immune checkpoint inhibition in non-small-cell lung cancer. *J Clin Oncol*. 2022;40(17):1916-1928.

doi: 10.1200/JCO.21.02010

31. Kearney CJ, Vervoort SJ, Hogg SJ, *et al*. Tumor immune evasion arises through loss of TNF sensitivity. *Sci Immunol*. 2018;3(23):e aar3451.

doi: 10.1126/sciimmunol.aar3451

32. Krummel MF, Mahale JN, Uhl LFK, *et al*. Paracrine costimulation of IFN-γ signaling by integrins modulates CD8 T cell differentiation. *Proc Natl Acad Sci U S A*. 2018;115(45):11585-11590.

doi: 10.1073/pnas.1804556115

33. Yang H, Zhang Q, Xu M, *et al*. CCL2-CCR2 axis recruits tumor associated macrophages to induce immune evasion through PD-1 signaling in esophageal carcinogenesis. *Mol Cancer*. 2020;19(1):41.

doi: 10.1186/s12943-020-01165-x